THE REFLECTION COEFFICIENT OF A GROUND-PLANE MOUNTED TEM MODE PARALLEL-PLATE WAVEGUIDE ILLUMINATING A CONDUCTING SHEET

L. L. Tsai and R. C. Rudduck

The Ohio State University
ElectroScience Laboratory
(formerly Antenna Laboratory)
Department of Electrical Engineering
Columbus, Ohio 43212

TECHNICAL REPORT 1691-27
24 May 1968

Grant Number: NsG-448

National Aeronautics and Space Administration
Office of Grants and Research Contracts
Washington, D.C. 20546

NOTICES

When Government drawings, specifications, or other data are used for any purpose other than in connection with a definitely related Government procurement operation, the United States Government thereby incurs no responsibility nor any obligation whatsoever, and the fact that the Government may have formulated, furnished, or in any way supplied the said drawings, specifications, or other data, is not to be regarded by implication or otherwise as in any manner licensing the holder or any other person or corporation, or conveying any rights or permission to manufacture, use, or sell any patented invention that may in any way be related thereto.

The Government has the right to reproduce, use, and distribute this report for governmental purposes in accordance with the contract under which the report was produced. To protect the proprietary interests of the contractor and to avoid jeopardy of its obligations to the Government, the report may not be released for non-governmental use such as might constitute general publication without the express prior consent of The Ohio State University Research Foundation.

REPORT

by

The Ohio State University ElectroScience Laboratory
(Formerly Antenna Laboratory)
Columbus, Ohio 43212

Sponsor	National Aeronautics and Space Administration Office of Grants and Research Contracts Washington, D.C. 20546
Grant Number	NsG-448
Investigation of	Spacecraft Antenna Problems
Subject of Report	The Reflection Coefficient of a Ground-Plane Mounted TEM Mode Parallel-Plate Waveguide Illuminating a Conducting Sheet
Submitted by	L.L. Tsai and R.C. Rudduck ElectroScience Laboratory Department of Electrical Engineering
Date	24 May 1968

ABSTRACT

The TEM mode reflection coefficient is analyzed for a symmetric parallel-plate waveguide terminated in a ground plane and radiating into a perfectly reflecting sheet oriented normal to the guide axis. By using the wedge diffraction method the reflection from the conducting sheet is treated in terms of successive contributions or bounces that describe the interacting waves between the waveguide wedges and the reflector.

Each of these bounce waves can be resolved into component cylindrical waves. The scattering of each of these component cylindrical waves by the guide produces two subsequent cylindrical waves. These are: the geometrical optics component which results from reflection from the ground plane and the aperture component which represents the effect of the aperture in the ground plane. Thus the total reflection from the sheet is obtained by summing these iterative contributions. The results from this analysis are in good agreement with measurements and the Fourier transform analysis presented in Ref. 4.

The transmission between waveguides is a by-product of the reflecting sheet analysis. Calculated results are given for the transmission between two waveguides with each mounted in a ground plane and facing each other.

TABLE OF CONTENTS

THE REFLECTION COEFFICIENT OF A GROUND-PLANE MOUNTED TEM MODE PARALLEL-PLATE WAVEGUIDE ILLUMINATING A CONDUCTING SHEET

I. INTRODUCTION

The reflection coefficient of a TEM mode symmetric parallel-plate waveguide illuminating a perfectly conducting sheet oriented normal to the guide axis as shown in Fig. 1 has been analyzed by wedge diffraction techniques.[1,2] The analysis of this reflecting sheet problem gives insight into the basic diffraction behavior of small aperture antennas which radiate into overdense plasmas. This analysis is applicable for spacecraft reentry situations in which the plasma medium can be adequately modeled by a simple reflecting sheet.

For the half-plane guide, multiple interactions between the guide and the reflector are negligible hence the reflection coefficient was obtained by considering only one single bounce wave. For guides with wedge angles (WA) less than 70°-80°, the reflection coefficient was found by assuming that the interactions between the guide aperture and the reflecting sheet are bouncing plane waves and obtaining these interaction waves through a self consistency procedure. For the ground plane case (WA = 90°) and the large wedge angle case[2] the interacting waves were treated as successively bouncing cylindrical component

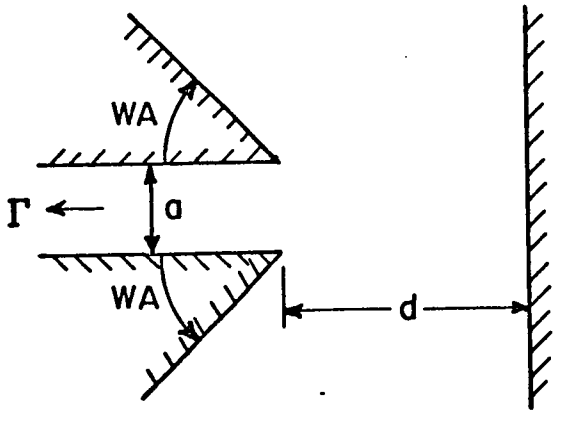

Fig. 1. Symmetric parallel-plate guide radiating into reflecting sheet.

waves. The total reflection coefficient in the ground plane case was obtained in Ref. 1 by summing the free space reflection coefficient, or that of the guide radiating in free space,[3] and the contribution of the first five bounce waves. Higher bounces were not included due to computational complexities.

Recently NASA engineers at Langley, Va. analyzed the same ground plane problem by using the Fourier Transform method with a dominant mode assumption.[4] Comparison of their results and that obtained in Ref. 1 indicated that effects of the higher order bounce waves are significant, especially when the spacing between the ground plane and reflecting sheet were near multiples of half wavelengths. In this report appropriate simplifications are made in the diffraction method analysis of Ref. 1 for ground-plane guides to allow the inclusion of up to several hundred higher order bounce waves. In fact, the summation is carried on until contributions from subsequent higher order bounces are indeed negligible.

A by-product of the analysis for the reflecting sheet problem is the solution to a different problem: the transmission between identical waveguides. In the transmission problem the sum of the odd-numbered bounces for the reflecting sheet problem gives the transmission to the receiving guide whereas the even-numbered bounces give the reflection coefficient of the transmitting guide. The sum of the transmitted and reflected waves in the transmission problem is equal to the reflected wave for the reflecting sheet problem. Calculated results are presented for the transmission between ground-plane mounted guides.

The free-space reflection coefficient for the ground-plane mounted TEM parallel plate waveguide[3] is given by

$$\Gamma_S = \frac{1}{2}\frac{\sqrt{\lambda}}{a}\left[D_1(\psi_1 = 0) + D_2(\psi_2 = 0) \right] e^{-j\frac{\pi}{4}}, \tag{1}$$

where

$$D_1(\psi_1 = 0) = D_2(\psi_2 = 0) = \frac{e^{-j\frac{\pi}{4}}}{\sqrt{2\pi k}} \left[R_1^{(1)}(\theta = -\pi) + R_1^{(2)}(\theta = -\pi) \right]$$

with

$$R_I^{(1)}(\theta) = \frac{1}{n} \sin \frac{\pi}{n} \left[\frac{1}{\cos \frac{\pi}{n} - \cos\left(\frac{\pi+\theta}{n}\right)} \right] ,$$

and

$$R_1^{(2)}(\theta) = R_1^{(1)}\left(\frac{\pi}{2}\right) \left[V_B\left(a, \frac{\pi}{2} - \theta, n\right) + V_B\left(a, \frac{3\pi}{2} - \theta, n\right) \right] .$$

II. REFLECTION COEFFICIENT ANALYSIS FOR THE GROUND-PLANE MOUNTED GUIDE

By the wedge diffraction method the reflection coefficient of the waveguide is the superposition of the free space reflection coefficient and the reflection coefficient caused by the presence of the conducting sheet. Formulating the reflection from the sheet in terms of successive bounces, the first bounce wave is the free space radiation from the waveguide which reflects from the sheet back onto the waveguide. The first bounce wave then scatters from the waveguide wedges producing a second bounce wave which propagates toward the reflecting sheet. The second bounce wave in turn reflects from the sheet back onto the waveguide giving rise to a third bounce wave, and so on to higher order bounces. Each bounce produces a contribution to the reflected TEM mode in the waveguide.

A. On-Axis Field of the TEM Mode Ground-Plane Mounted Guide as the First Bounce Wave

Calculations of the free space fields of various parallel-plate guides has been made[1,6] using the near field formulation outlined in Ref. 5. These calculations show that in the region of the projected guide cross section the free space wave radiated from the guide may be represented by an isotropic cylindrical wave from a line source. The line source location may be determined exactly by examining the phase curvature as was done in Ref. 1. In general, however, the line source may be assumed to be located at the center of the guide aperture to a very good degree of approximation.[6]

This and subsequent approximations in the analysis are valid provided the observation distances are sufficiently removed from the aperture. For guidewidths (a) less than a wavelength this minimum distance, which is dependent on the guide width, is less than a wavelength. Because of this limitation in the general analysis, the conducting sheet is required to be sufficiently removed from the aperture for the analysis to be valid. For example, for a guide width equal to 0.278λ the minimum distance (d) is approximately 0.5λ.

The equivalent cylindrical wave for the first bounce wave is given by the free space field on the axis of the guide; this field as analyzed by wedge diffraction may be obtained by summing the singly and doubly diffracted fields as shown in Fig. 2. The singly diffracted wave from edges 1 and 2 expressed in ray form are given respectively by

$$R_1^{(1)}(\theta) = \frac{1}{n} \sin\frac{\pi}{n} \left(\frac{1}{\cos\frac{\pi}{n} - \cos\frac{\pi+\theta}{n}} \right) , \tag{2}$$

and

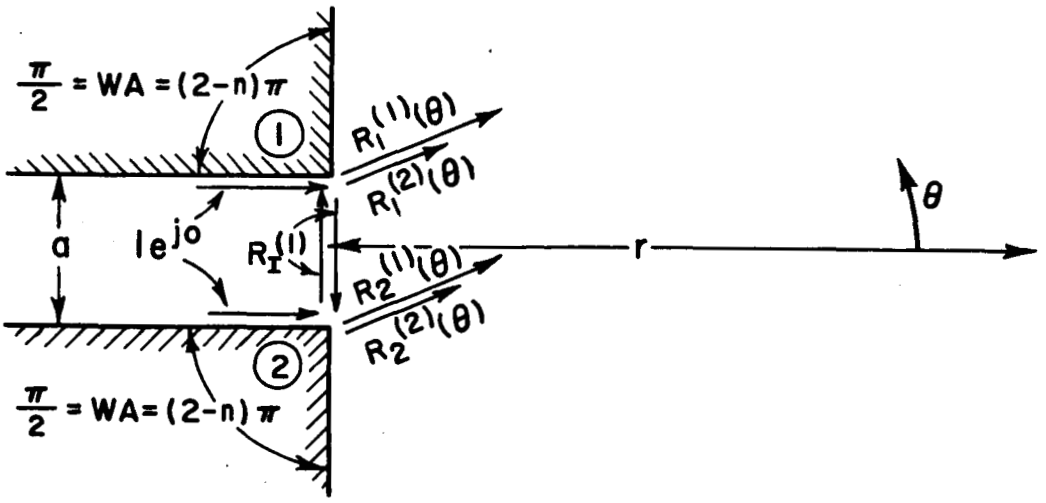

Fig. 2. Singly and doubly diffracted rays from the guide.

$$(3) \qquad R_2^{(1)}(\theta) = \frac{1}{n} \sin\frac{\pi}{n} \left(\frac{1}{\cos\frac{\pi}{n} - \cos\frac{\pi - \theta}{n}} \right) e^{jka\sin\theta} ,$$

where the exponential term in Eq. (3) results from referring the phase to edge 1.

The singly diffracted ray which illuminates the opposite edge giving rise to the doubly diffracted waves is given by

$$(4) \qquad R_I^{(1)} = \frac{1}{n} \sin\frac{\pi}{n} \left(\frac{1}{\cos\frac{\pi}{n} - \cos\frac{\pi/2}{n}} \right) .$$

The doubly diffracted ray is then given by

$$(5) \qquad R_1^{(2)} = R_I^{(1)} \left[V_B\left(a, \frac{\pi}{2} + \theta, n\right) + V_B\left(a, \frac{3\pi}{2} + \theta, n\right) \right]$$

$$(6) \qquad R_2^{(2)} = R_I^{(1)} \left[V_B\left(a, \frac{\pi}{2} - \theta, n\right) + V_B\left(a, \frac{3\pi}{2} - \theta, n\right) \right] e^{-jka\sin\theta} .$$

The total radiation from the guide is then

$$(7) \qquad R_T(\theta) = R_1^{(1)}(\theta) + R_2^{(1)}(\theta) + R_1^{(2)}(\theta) + R_2^{(2)}(\theta) .$$

The on-axis field radiated by the guide is then obtained by taking the limit on $R_T(\theta)$ as $\theta \to 0$ and is given by

$$(8a) \qquad H_T(r, \theta=0) = \left[\lim_{\theta \to 0} R_T(\theta) \right] \frac{e^{-j\left(kr + \frac{\pi}{4}\right)}}{\sqrt{2\pi kr}}$$

$$= \left[jka - \frac{1}{1.5} \cot\frac{\pi}{1.5} + 2R_I^{(2)} \right] \frac{e^{-j\left(kr + \frac{\pi}{4}\right)}}{\sqrt{2\pi kr}} ,$$

where

$$R_I^{(2)} = R_1^{(2)}(\theta=0) = R_2^{(2)}(\theta=0)$$

$$= R_I^{(1)} \left[V_B\left(a, \frac{\pi}{2}\right) + V_B\left(a, \frac{3\pi}{2}\right) \right] \quad . \tag{8b}$$

The relationship expressed in Eq. (8) may also be obtained by performing the limit operation on the near-zone field expressions found in Ref. 1 as will be discussed in a later report.[6] The first bounce wave is then simply expressed as an isotropic cylindrical wave with field values given by Eq. (8).

B. Multiple Bounce Formulation

For purposes of determining the second bounce wave in the projected guide cross section, the first bounce wave may be treated as that of an isotropic cylindrical wave from a line source located at a distance 2d from the guide aperture, where d is the distance to the sheet as shown in Fig. 3a. The scattering of a cylindrical wave by the wedges forming the waveguide may be analyzed by the wedge diffraction method. Calculations show that the scattered wave can be resolved into two cylindrical wave components.[1] The principal component is the geometrical optics component or the reflection of the incident cylindrical wave by the ground plane without an aperture. This wave component has a virtual source located at the image in the ground plane of the equivalent line source representing the first bounce wave as shown in Fig. 3b. The second component is the aperture component which is the difference between the total second bounce wave and the geometrical optics component. The aperture component is very similar to the backscatter by a strip or thick wall. Calculations show that in the region of the projected guide cross section the aperture component may be represented by an isotropic cylindrical wave with its source located at the center of the aperture,[1] as shown in Fig. 3c.

The aperture component of the scattered field resulting from an incident cylindrical wave depends only on the value of the incident field and is independent of the source location provided the source is sufficiently removed from the guide, as discussed previously. This fact together with a shadow boundary approximation for the wedge diffraction function V_B permits the value of the aperture component to be simply computed. The

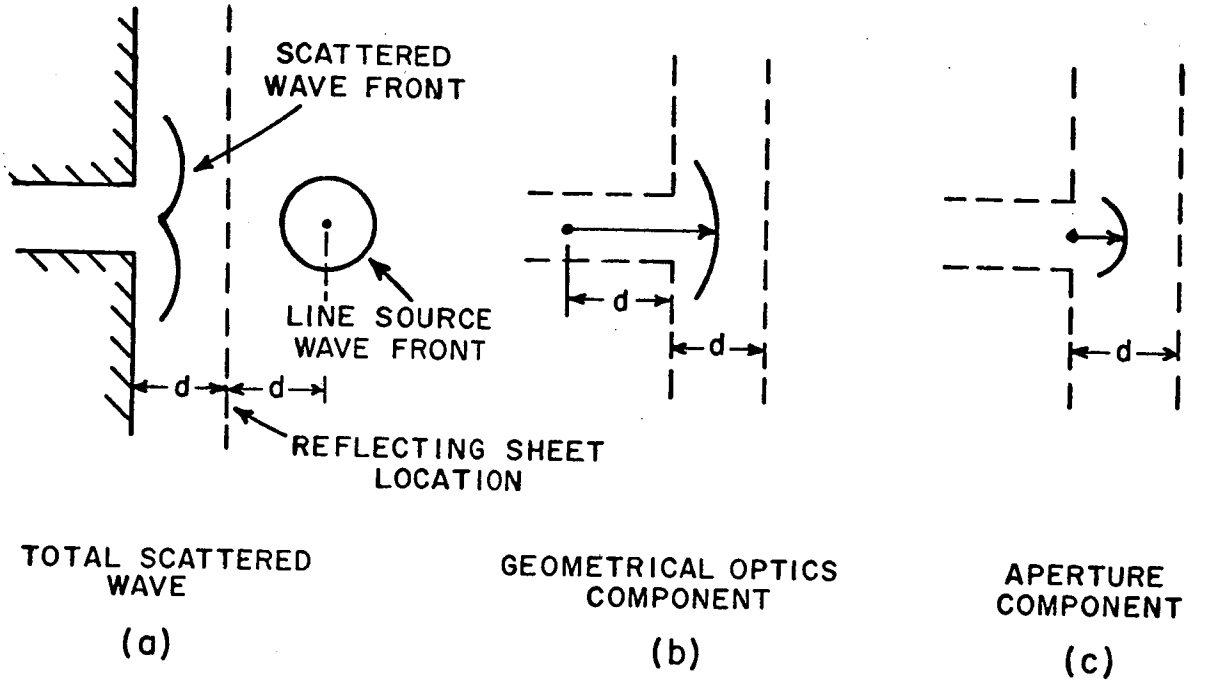

Fig. 3. Scattering of a cylindrical wave in the ground plane case.

simplification results because the aperture component may be determined using plane wave diffraction from the waveguide wedges.

For a plane wave of unit magnitude normally incident on the waveguide wedges as shown in Fig. 4 the diffracted field at a point P is given by

$$H(P) = V_B\left(r_1, \psi_1 + \frac{\pi}{2}\right) + V_B\left(r_2, \psi_2 + \frac{\pi}{2}\right) + V_B\left(r_1, \psi_1 - \frac{\pi}{2}\right) + V_B\left(r_2, \psi_2 - \frac{\pi}{2}\right) + D_o^{(1)}\left[U_d(r_1, a, \psi_1, \pi) + U_d(r_2, a, \psi_2, \pi)\right] \tag{9}$$

where

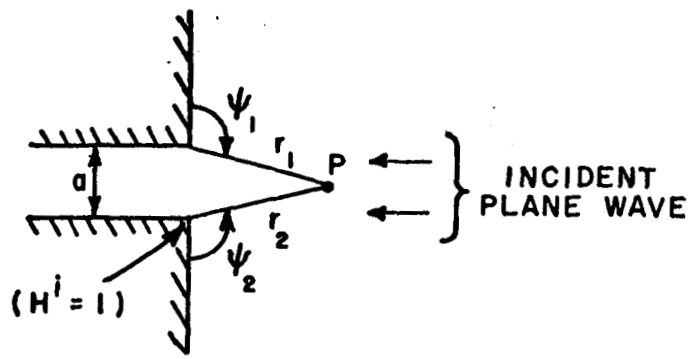

Fig. 4. Scattering of an incident plane wave in the ground plane case.

$$(10) \qquad D_o^{(1)} = \frac{2}{3}\sin\frac{2}{3}\pi \left[\left(\cos\frac{2}{3}\pi - \cos\frac{\pi}{3}\right)^{-1} + \left(\cos\frac{2}{3}\pi - \cos\pi\right)^{-1}\right]\frac{e^{-j\frac{\pi}{4}}}{\sqrt{2\pi k}}$$

corresponds to the singly diffracted ray from each edge which illuminates the opposite edge and

$$(11) \qquad U_d(r, r_o, \psi, \psi_o) = \frac{e^{-jk(r+r_o)}}{\sqrt{r+r_o}} \; e^{jk\left(\frac{r\, r_o}{r+r_o}\right)} \cdot \left[V_B\left(\frac{r\, r_o}{r+r_o}, \psi-\psi_o\right) + V_B\left(\frac{r\, r_o}{r+r_o}, \psi+\psi_o\right)\right]$$

is the diffracted field at (r, ψ) due to a line source at (r_o, ψ_o)[5]. The V_B terms in Eq. (9) result from the singly diffracted waves from the wedges whereas the U_d terms express the doubly diffracted waves.

The terms $V_B(r, \psi \pm \pi/2)$ are given by the Fresnel integral formulation of Hutchins and Kouyoumjian[8,9] in which the Fresnel functions can be approximated in the region corresponding to the projected guide cross section by

(12) $C(W) \cong W$ for W small.

$S(W) \cong O$

Thus a shadow boundary approximation for V_B is obtained as shown in Appendix III and is given by

(13) $$V_B(r,\phi) \cong \frac{1}{2}\exp(jkr\cos\phi) \times \left\{ \pm \left[1 - 4\, e^{j\frac{\pi}{4}} \sqrt{\frac{r}{\lambda}} \left| \cos\frac{\phi}{2} \right| \right] - \frac{1}{n}\cot\frac{\pi}{n} \frac{e^{-j\frac{\pi}{4}}}{\sqrt{2\pi kr}} \right\}$$

for $\phi \cong \pi$

where the + sign is for $\phi > \pi$ and the minus sign is for $\phi < \pi$. For the ground plane mounted guide (90° wedge angle = $(2-n)\pi$ = interior wedge angle), $\phi > \pi$ and $n = 1.5$.

The following approximation is also valid in the projected guide cross section:

(14) $$\cos\frac{1}{2}\left(\psi_1 + \frac{\pi}{2}\right) + \cos\frac{1}{2}\left(\psi_2 + \frac{\pi}{2}\right) \cong -\frac{a}{2r_o} \quad .$$

Thus in the region of the projected guide cross section the first two terms in Eq. (9) may be approximated as

(15) $$V_B\left(r_1, \psi_1 + \frac{\pi}{2}\right) + V_B\left(r_2, \psi_2 + \frac{\pi}{2}\right)$$

$$= \exp(jkr_o\cos\phi_o) \left[1 + 2\, e^{j\frac{\pi}{4}} \sqrt{\frac{r}{\lambda}} \left(\cos\frac{\psi_1 + \frac{\pi}{2}}{2} + \cos\frac{\psi_2 + \frac{\pi}{2}}{2} \right) - \frac{1}{n}\cot\frac{\pi}{n} \frac{e^{-j\frac{\pi}{4}}}{\sqrt{2\pi kr}} \right]$$

$$= \exp(jkr_o\cos\phi_o) \left[1 - \frac{a}{\sqrt{\lambda r_o}}\, e^{j\frac{\pi}{4}} - \frac{1}{n}\cot\frac{\pi}{n} \frac{e^{-j\frac{\pi}{4}}}{\sqrt{2\pi kr_o}} \right]$$

where r_o and ϕ_o are the coordinates of the observation point P with respect to the center of the aperture and hence

$$(16) \qquad r_o \cos\phi_o = r_1 \cos\left(\psi_1 + \frac{\pi}{2}\right) = r_2 \cos\left(\psi_2 + \frac{\pi}{2}\right) \quad .$$

The term $\exp(jkr_o \cos\phi_o)$ in Eq. (15) is identified as the reflected plane wave from the ground plane without the waveguide aperture present and hence corresponds to the geometrical optics component of the scattered field for plane wave incidence. The second two terms in Eq. (15) together with the $V_B(r, \psi-\pi/2)$ and $D_o^{(1)}$ U_d terms of Eq. (9) constitute the aperture component of the plane wave diffraction. For the $V_B(r, \psi-\pi/2)$ terms the asymptotic form valid for large values of $kr[1 + \cos(\psi - \pi/2)]$ may be used:

$$(17) \qquad V_B\left(r, \psi - \frac{\pi}{2}\right) = \frac{\frac{2}{3}\sin\frac{2}{3}\pi}{\cos\frac{2}{3}\pi - \cos\frac{2}{3}\left(\psi - \frac{\pi}{2}\right)} \frac{e^{-j\left(kr + \frac{\pi}{4}\right)}}{\sqrt{2\pi kr}}$$

For the case of cylindrical wave incidence as shown in Fig. 3 the aperture component of the scattered wave is, to a very good approximation, the same as that for plane wave incidence shown in Fig. 4, with the plane wave field equal to the incident field of the cylindrical wave at the waveguide aperture. Thus the aperture component for cylindrical wave incidence is obtained from Eqs. (15) and (17) as

$$(18a) \qquad H_A = H^i K_A \frac{e^{-jkr_o}}{\sqrt{r_o}} \quad ,$$

and

$$(18b) \qquad K_A = \left[-\frac{a}{\sqrt{\lambda}} e^{j\frac{\pi}{4}} - \frac{2}{9\pi}\sqrt{3\lambda}\, e^{-j\frac{\pi}{4}} - \frac{1}{1.5}\cot\frac{\pi}{1.5}\right] \frac{e^{-j\frac{\pi}{4}}}{\sqrt{2\pi k}}$$

$$+ 2\, D_o^{(1)}\left[V_B\left(a, \frac{\pi}{2}\right) + V_B\left(a, \frac{3\pi}{2}\right)\right] \quad ,$$

where H^i is the incident field of the cylindrical wave at the aperture.

Since the first bounce wave can be adequately described by an isotropic line source at the center of the aperture of the waveguide image, the first bounce contribution to the reflection coefficient is obtained as shown in Fig. 5a. The modal current induced in the waveguide by a line source I_1 is given by (Ref. 5, Eq. (18))

$$(19a) \qquad I = \sqrt{\frac{\lambda}{2\pi a}}\, H_T(\Omega)\, I_1 ,$$

and

$$(19b) \qquad I_1 = \left(jka - \frac{1}{1.5} \cot \frac{\pi}{1.5} + 2R_I^{(2)} \right) \frac{e^{-j\frac{\pi}{2}}}{\sqrt{k}} ,$$

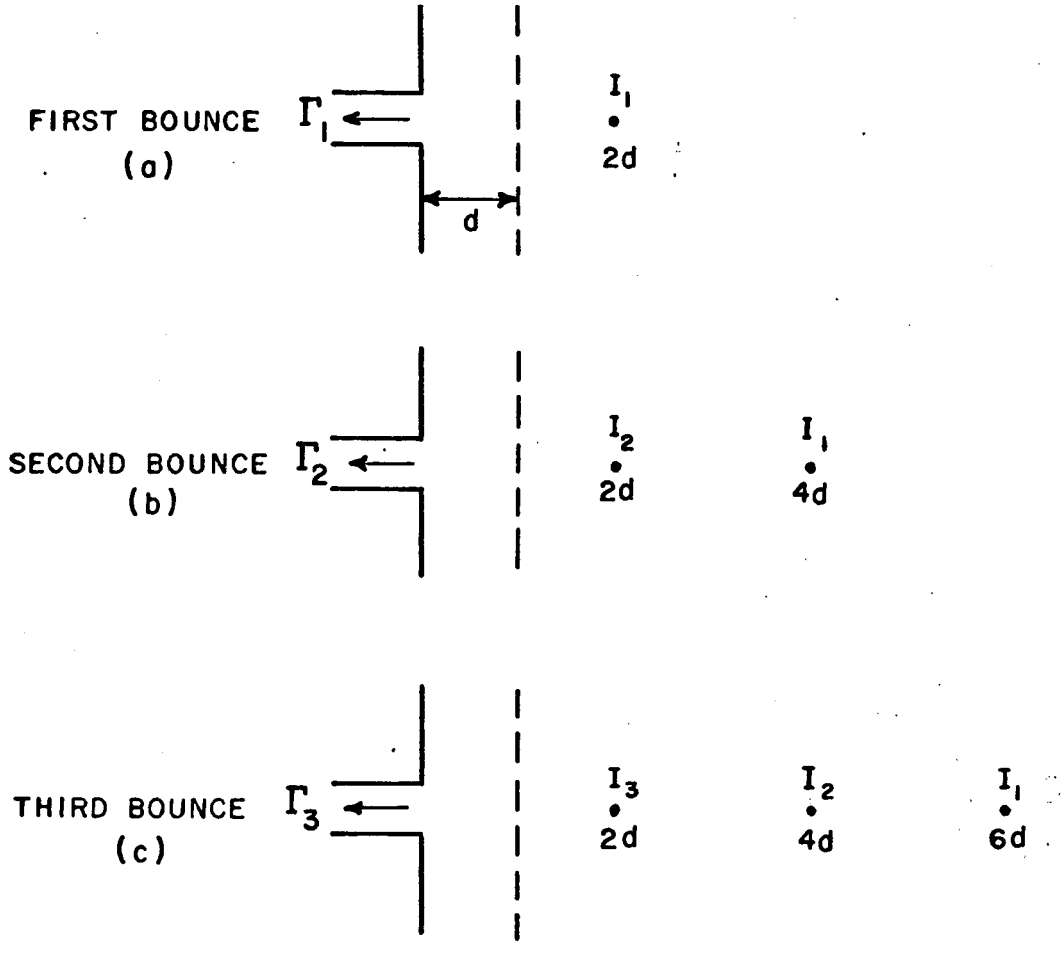

Fig. 5. Bounce contributions to reflection coefficient.

where $H_T(Q)$ is the free space magnetic field at point Q as radiated from the guide with an incident modal current $\sqrt{a}$ from within the guide. The line source I_1 radiates the on-axis field of the waveguide as given by Eq. (8). Using the value of $H_T(Q)$ as given by Eq. (8) the first bounce reflection coefficient is obtained from Eq. (19) as

$$\Gamma_1 = \frac{I}{\sqrt{a}} = C\, I_1 \frac{e^{-jk(2d)}}{\sqrt{2d}} \tag{20}$$

where

$$C = \frac{e^{j\frac{\pi}{4}}}{\sqrt{2\pi}} \left[1 + \left(\frac{1}{jka}\right)\left(\frac{-1}{1.5}\cot\frac{\pi}{1.5} + 2\, R_I^{(2)}\right)\right] \tag{21}$$

and $R_I^{(2)}$ is given by Eq. (8b).

The scattering of the cylindrical wave from I_1 by the waveguide results in a second bounce wave which is composed of two components as shown in Fig. 3. The geometrical optics component of the second bounce wave reflects from the sheet back onto the waveguide such that it may be represented by the line source I_1 located at a distance 4d from the guide aperture, as shown in Fig. 5b. The aperture component of the second bounce wave reflects onto the waveguide as described by the line source I_2 in Fig. 5b. The value of I_2 is obtained by equating the value of its radiated field with that of the aperture component in Eq. (18)

$$H_A = I_2 \frac{e^{-jkr_o + j\frac{\pi}{4}}}{\sqrt{2\pi r_o}} = H^i K_A \frac{e^{-jkr_o}}{\sqrt{r_o}} \,. \tag{22}$$

H^i is the incident field of the illuminating line source I_1 at the guide aperture in Fig. 5a, as given by

$$H^i = I_1 \frac{e^{-jk(2d) + j\frac{\pi}{4}}}{\sqrt{2\pi(2d)}} \,. \tag{23}$$

Hence the value of I_2 is given by

$$I_2 = I_1 K_A \frac{e^{-jk(2d)}}{\sqrt{2d}} \tag{24}$$

The corresponding second bounce reflection coefficient is then given by the modal current induced by I_1 and I_2 as shown in Fig. 5b:

$$\Gamma_2 = C\left[I_1 \frac{e^{-jk(4d)}}{\sqrt{4d}} + I_2 \frac{e^{-jk(2d)}}{\sqrt{2d}}\right] \quad . \tag{25}$$

The n-th bounce wave is given by n cylindrical wave components with sources: I_1 at n(2d), I_2 at (n-1)(2d), ..., I_n at 2d. The n-th source is given by

$$I_n = K_A \sum_{m=1}^{n-1} I_m \frac{e^{-jk2d(n-m)}}{\sqrt{2d(n-m)}} \tag{26}$$

and the n-th contribution to the reflection coefficient is given by

$$\Gamma_n = C \sum_{m=1}^{n} I_m \frac{e^{-jk2d(n-m+1)}}{\sqrt{2d(n-m+1)}} \quad . \tag{27}$$

The total reflection coefficient due to the reflecting sheet or plate is given by

$$\Gamma_p = \sum_{n=1}^{\infty} \Gamma_n \quad . \tag{28}$$

The total reflection coefficient Γ of the waveguide is obtained by superposing Γ_p and the free space reflection coefficient Γ_s:

$$\Gamma = \Gamma_s + \Gamma_p \, . \tag{29}$$

C. Results

The total reflection coefficient for the ground-plane mounted guide calculated by wedge diffraction analysis is compared to the results of the Fourier Transform solution[4] and to measured results in Figs. 6 through 18. Figures 6 and 7 shows the comparisons of the reflection

coefficient in both phase and magnitude for a ground-plane mounted guide with guide width equal to 0.278λ and with the reflector spacing (d) ranging from 0.5 to 2.0λ. The measured data in Fig. 6 was obtained using a narrow angle sectoral horn to simulate a parallel-plate waveguide.[1] Figures 8 and 9 show the comparison for the same guide with reflector spacing ranging from 2.0λ to 2.5λ and from 19.5λ to 20.0λ. For larger reflector spacing near 20λ the resonance behavior becomes much more localized as characterized by the sharp spike in the reflection coefficient at critical spacings.

The comparison for the guide width equal to 0.332λ case is shown in Figs. 10 and 11. Figures 12 and 13 compares the results for a 0.423λ guide width. In Figs. 10 and 12 the measured data were obtained by Jones and Swift[4] using an extremely narrow angle sectoral horn.

In Figs. 14, 15, and 16 the comparison is made for guides of widths equal to 0.6λ, 0.8λ, and 1.0λ, respectively, with reflector spacings ranging from 1.5λ to 2.0λ.

Figures 17 and 18 compares the two methods for guide width equal to 1.0λ and reflector spacing ranging from 4.5λ to 5.0λ and 19.5λ to 20.0λ, respectively.

As can be seen from the comparison, remarkably good agreement is found in general between the reflection coefficient calculated by the wedge diffraction method and that by the Fourier Transform method.

The larger differences found between the two methods for relatively small d/a may be attributed to inadequacies in the uniform line source approximation of the guide radiation in the wedge diffraction method. As d/a increases, the uniform line source assumption becomes quite good and the agreement between the two methods is seen to become much closer.

By the close agreement between the results for $d > 1.0\lambda$, the dominant mode assumption made in the Fourier Transform solution[4] can be concluded to be quite accurate since higher order mode effects are included in the wedge diffraction solution. Appendix IV gives both the free-space reflection coefficient and the on-axis guide radiation computed with and without the presence of higher order modes. This comparison shows that the presence of higher order modes affects the magnitudes of these quantities very little and only introduces a small phase correction. It is thus concluded that this higher order mode phase correction factor causes the small disagreement between the results obtained from the Fourier Transform and the wedge diffraction methods.

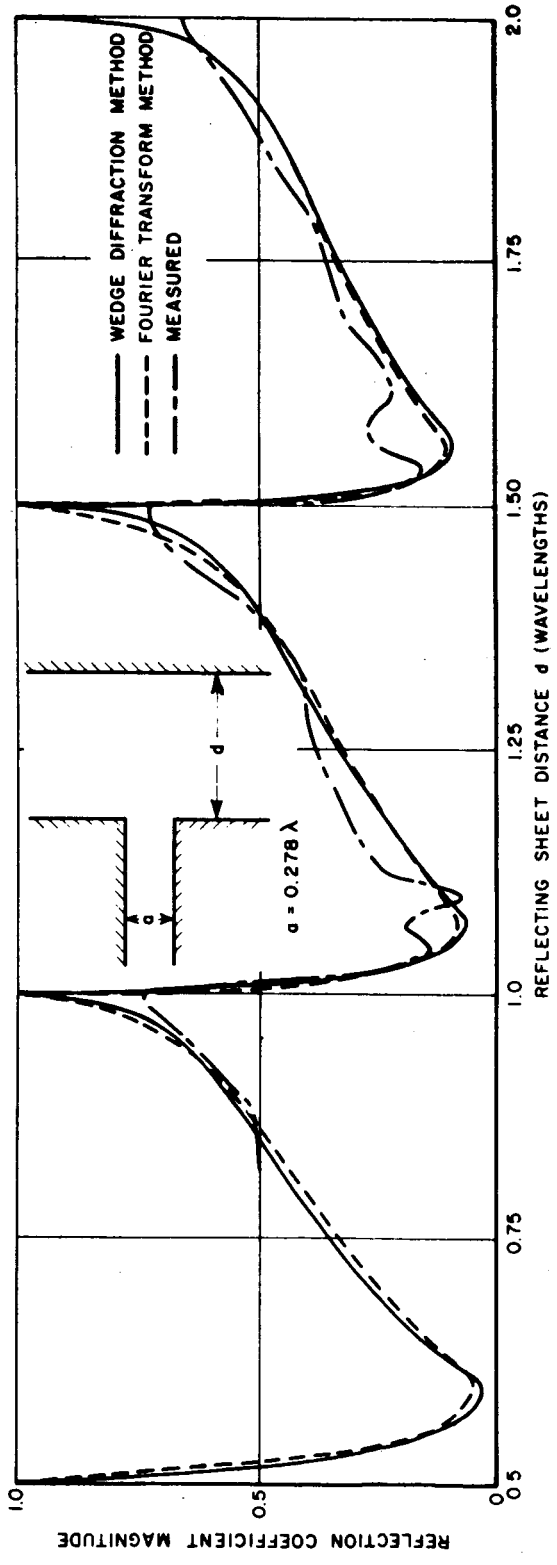

Fig. 6. The reflection coefficient magnitude comparison for a = 0.278λ.

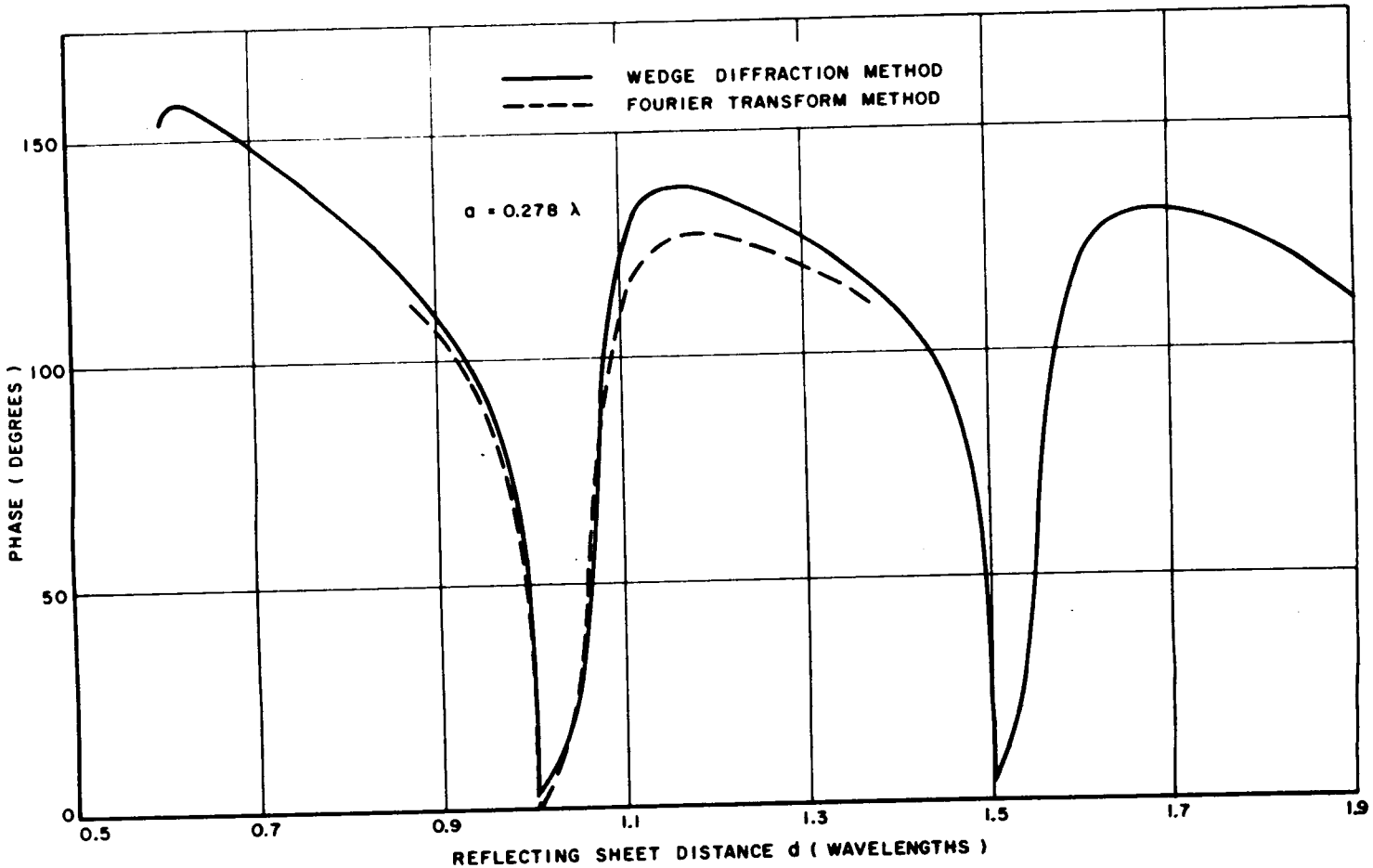

Fig. 7. The reflection coefficient phase comparison for a = 0.278λ.

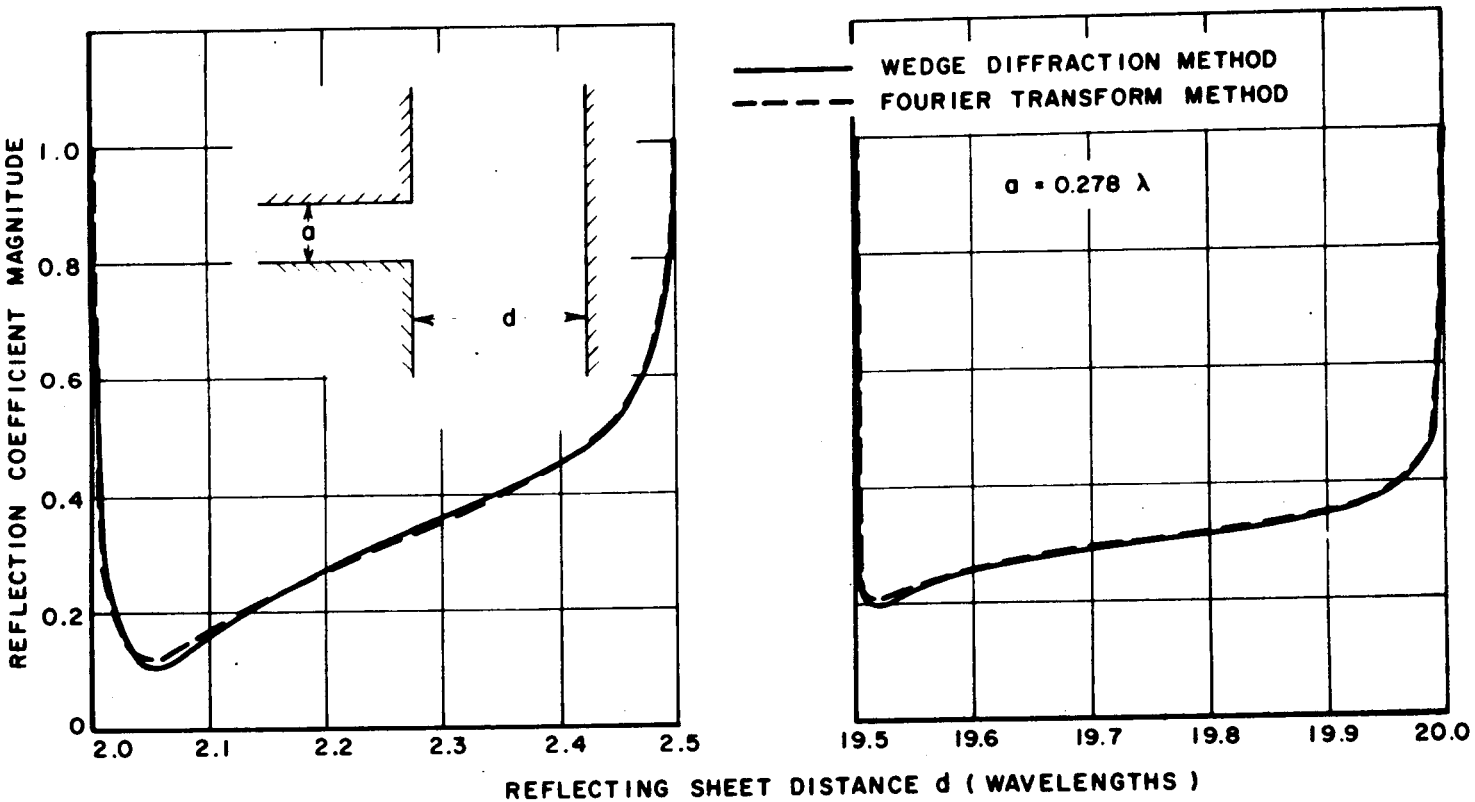

Fig. 8. Reflection coefficient magnitude for a = 0.278λ .

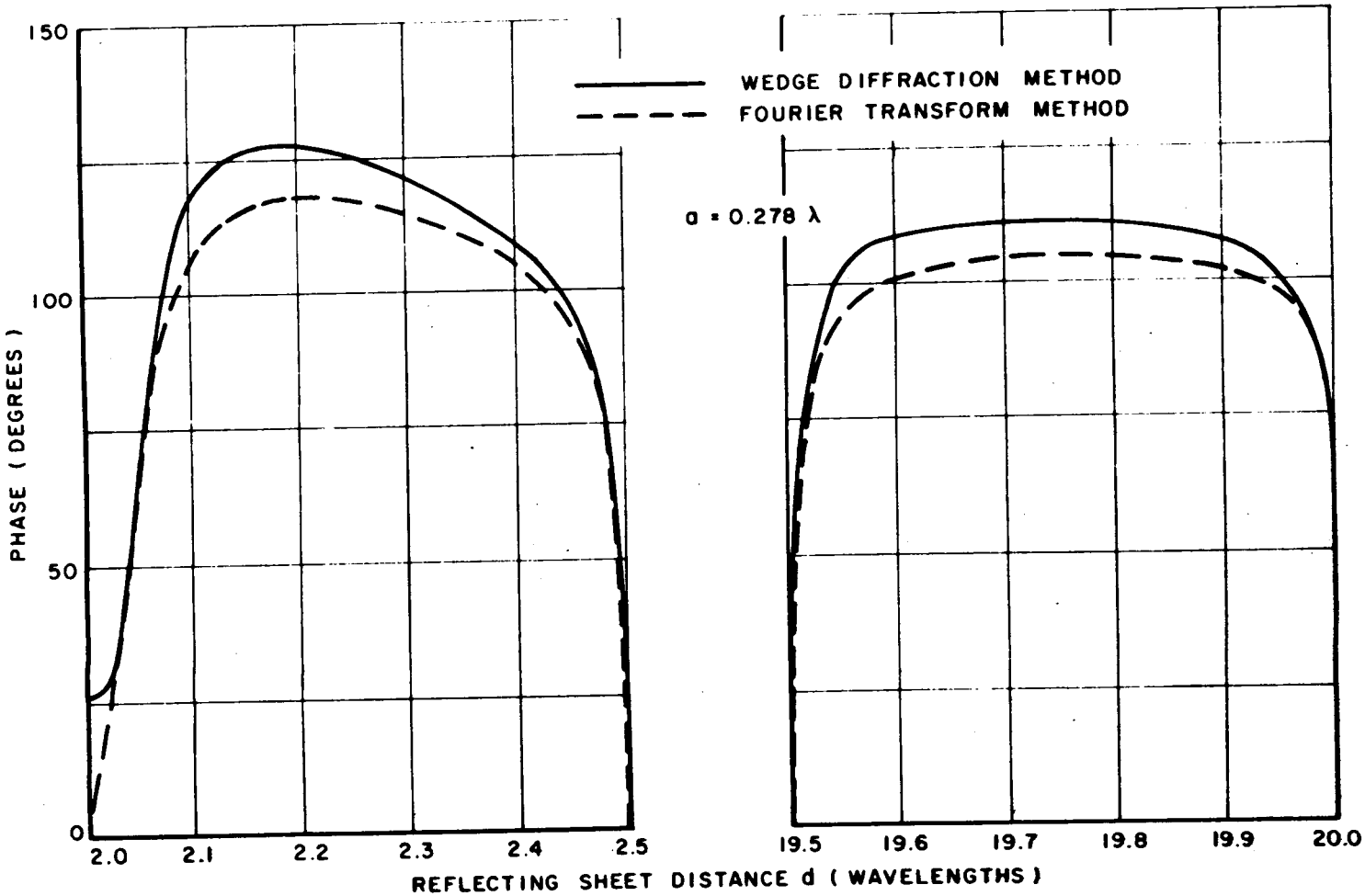

Fig. 9. Reflection coefficient phase for a = 0.278λ .

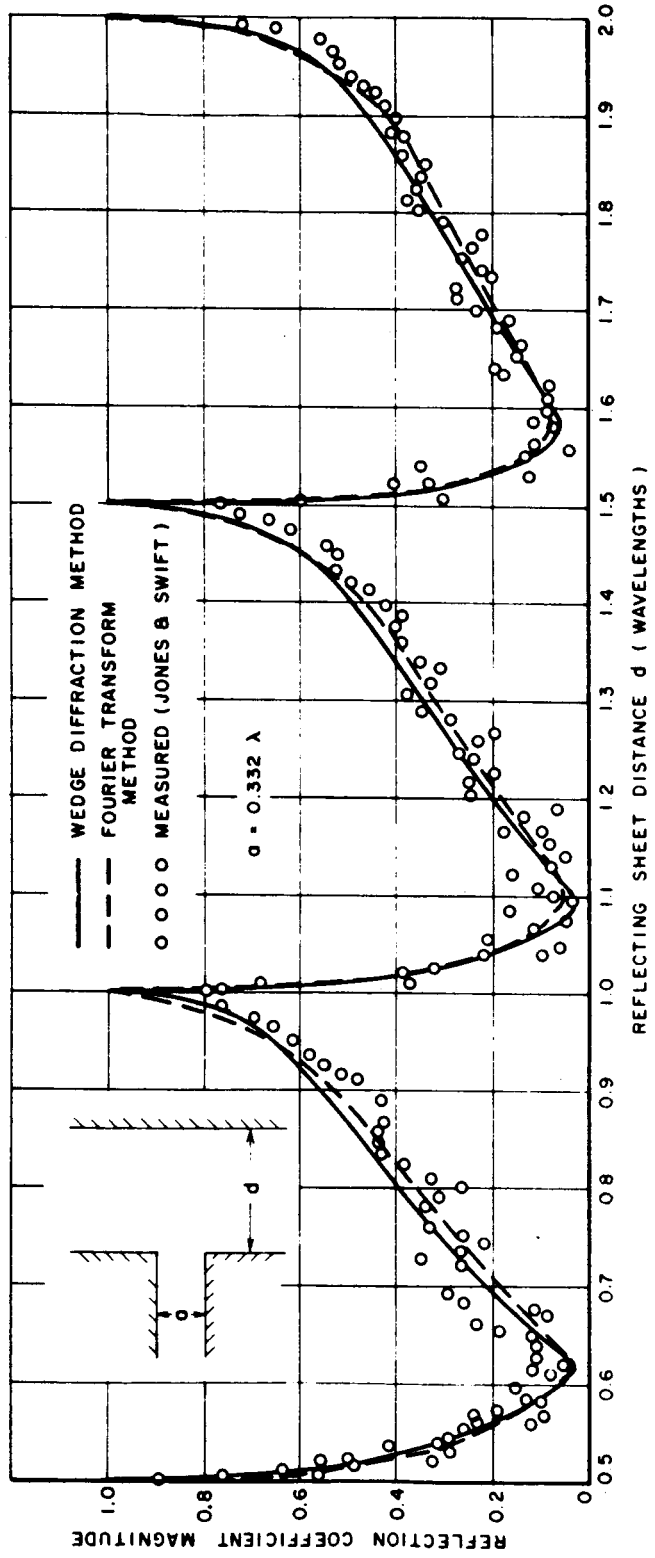

Fig. 10. Reflection coefficient magnitude comparison for a = 0.332λ.

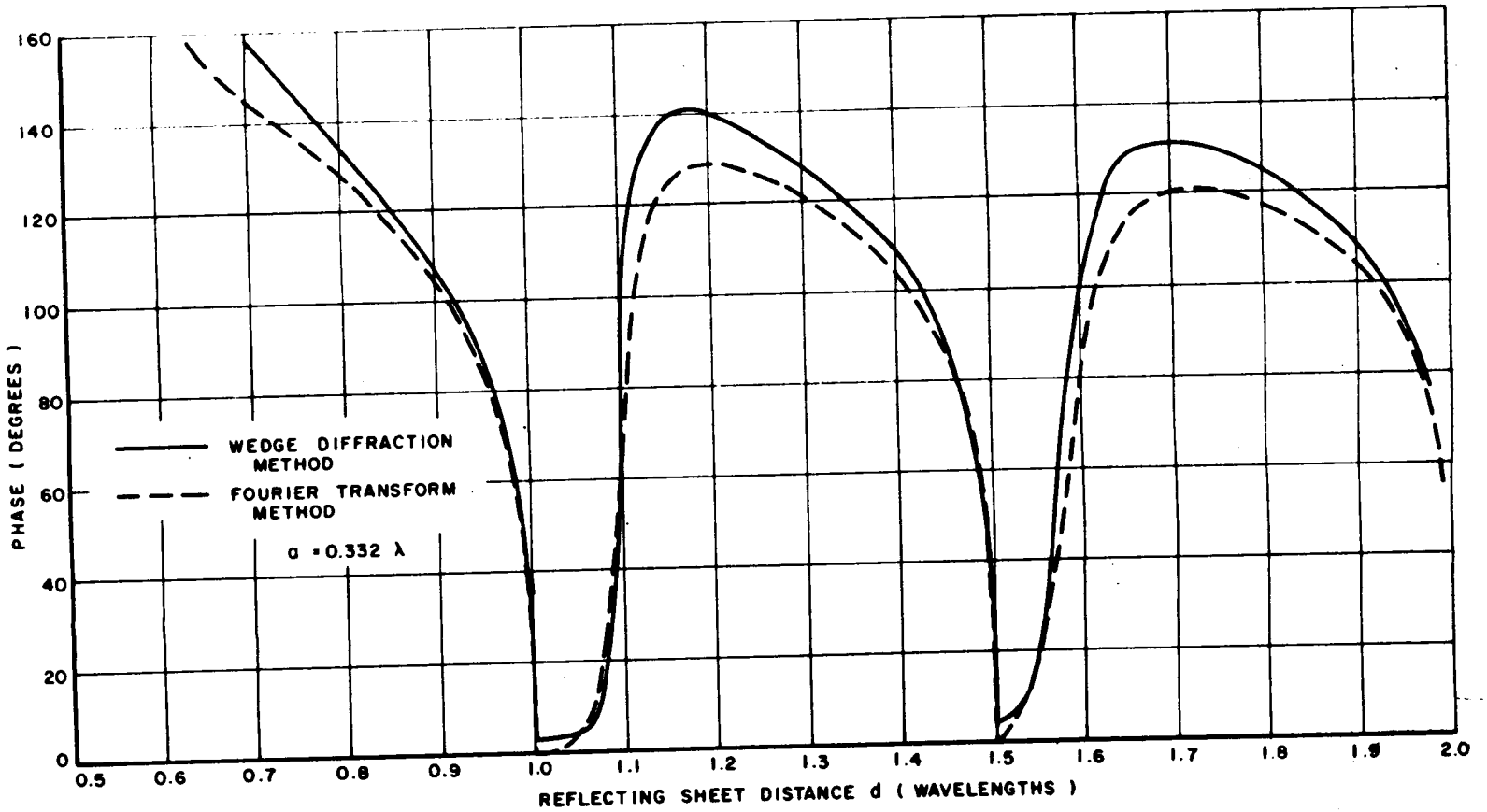

Fig. 11. Reflection coefficient phase comparison for a = 0.332λ .

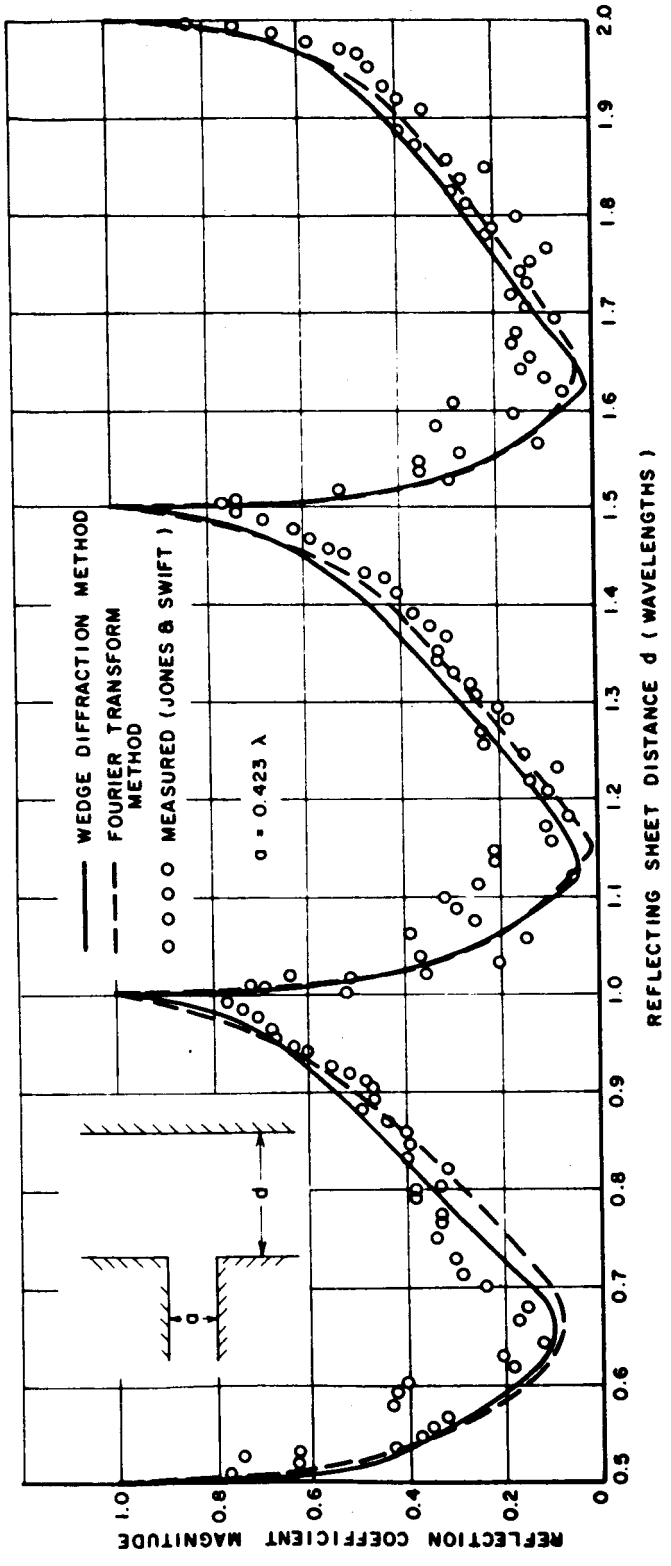

Fig. 12. Reflection coefficient magnitude comparison for a = 0.423λ.

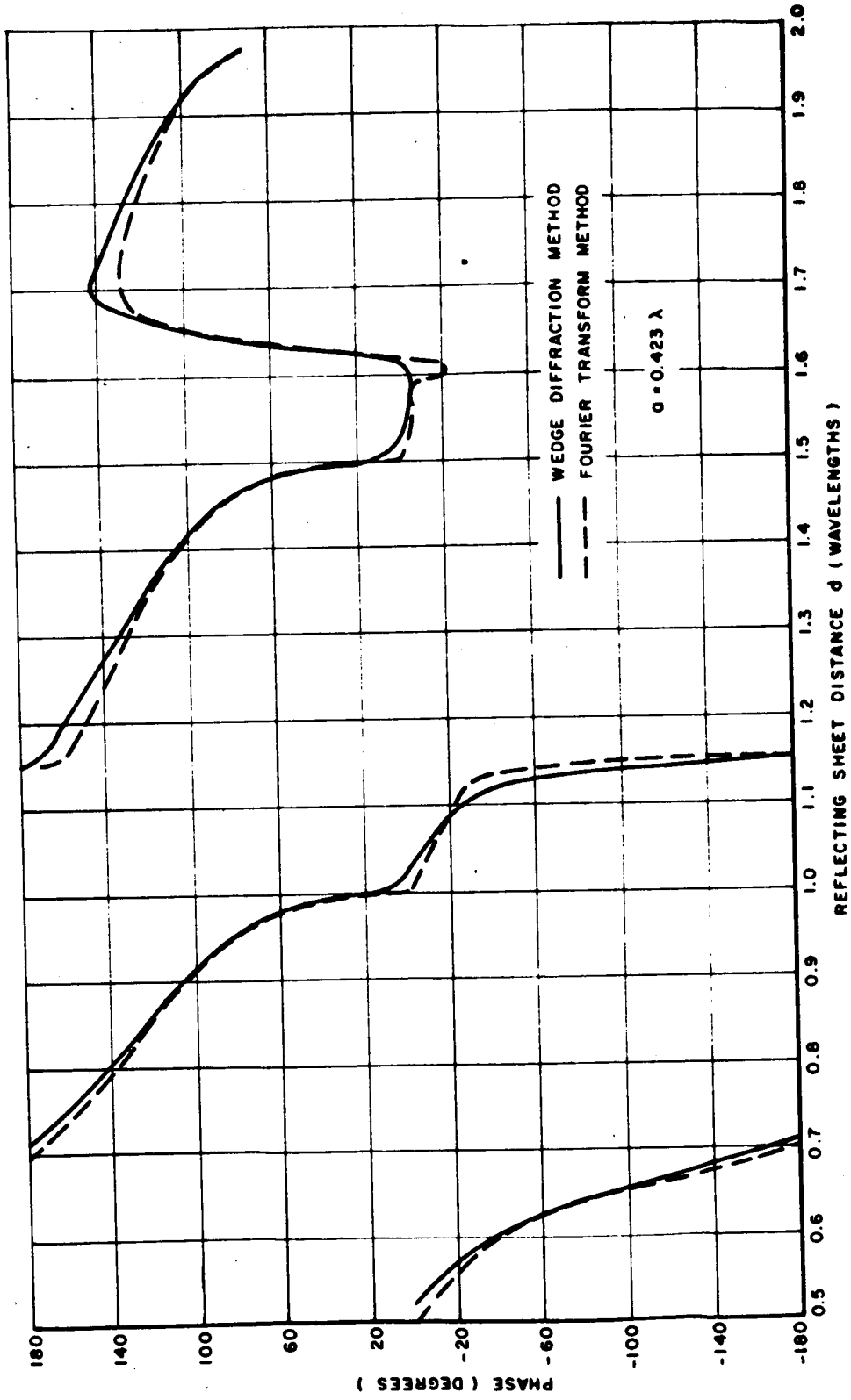

Fig. 13. Reflection coefficient phase comparison for a = 0.432λ.

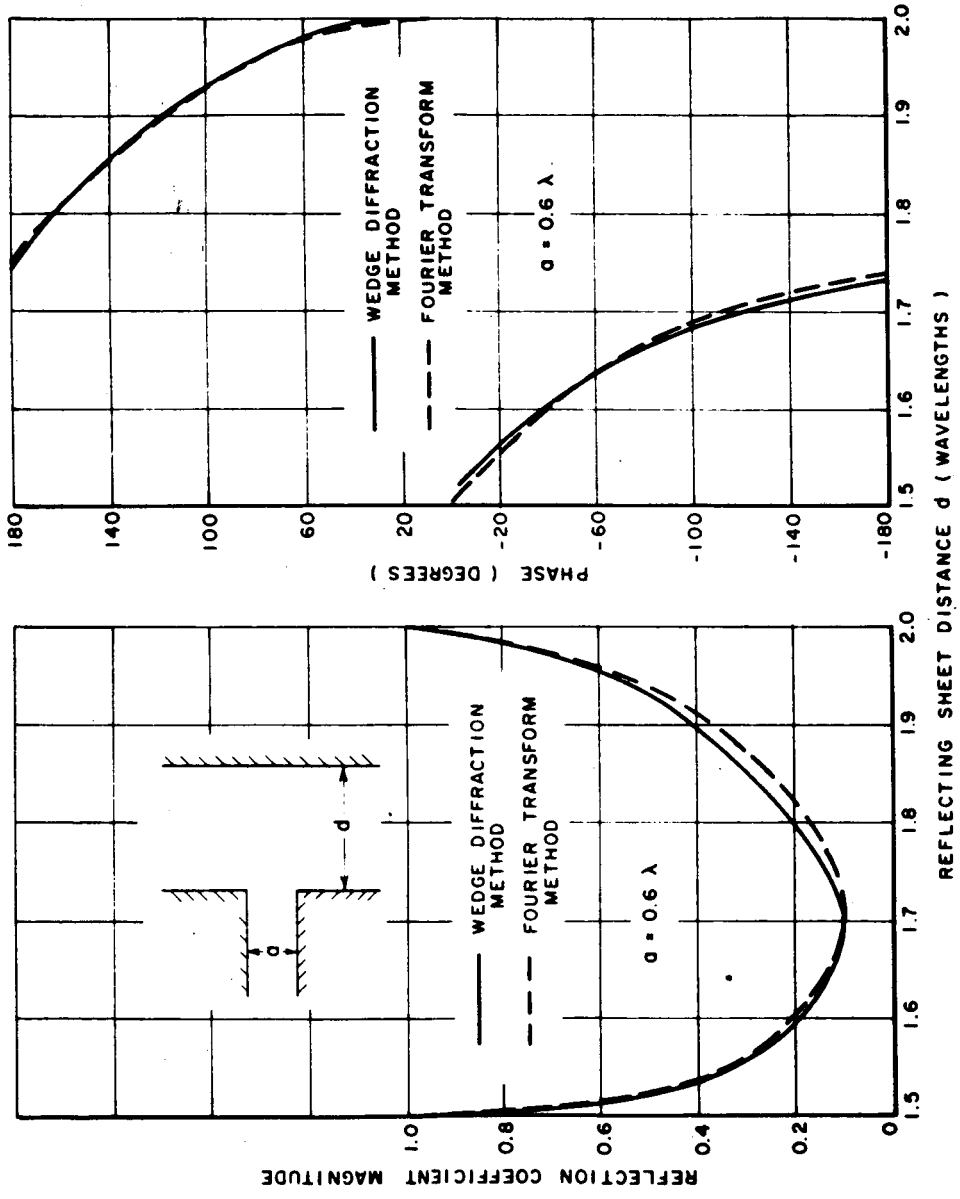

Fig. 14. Reflection coefficient comparison for a = 0.6λ.

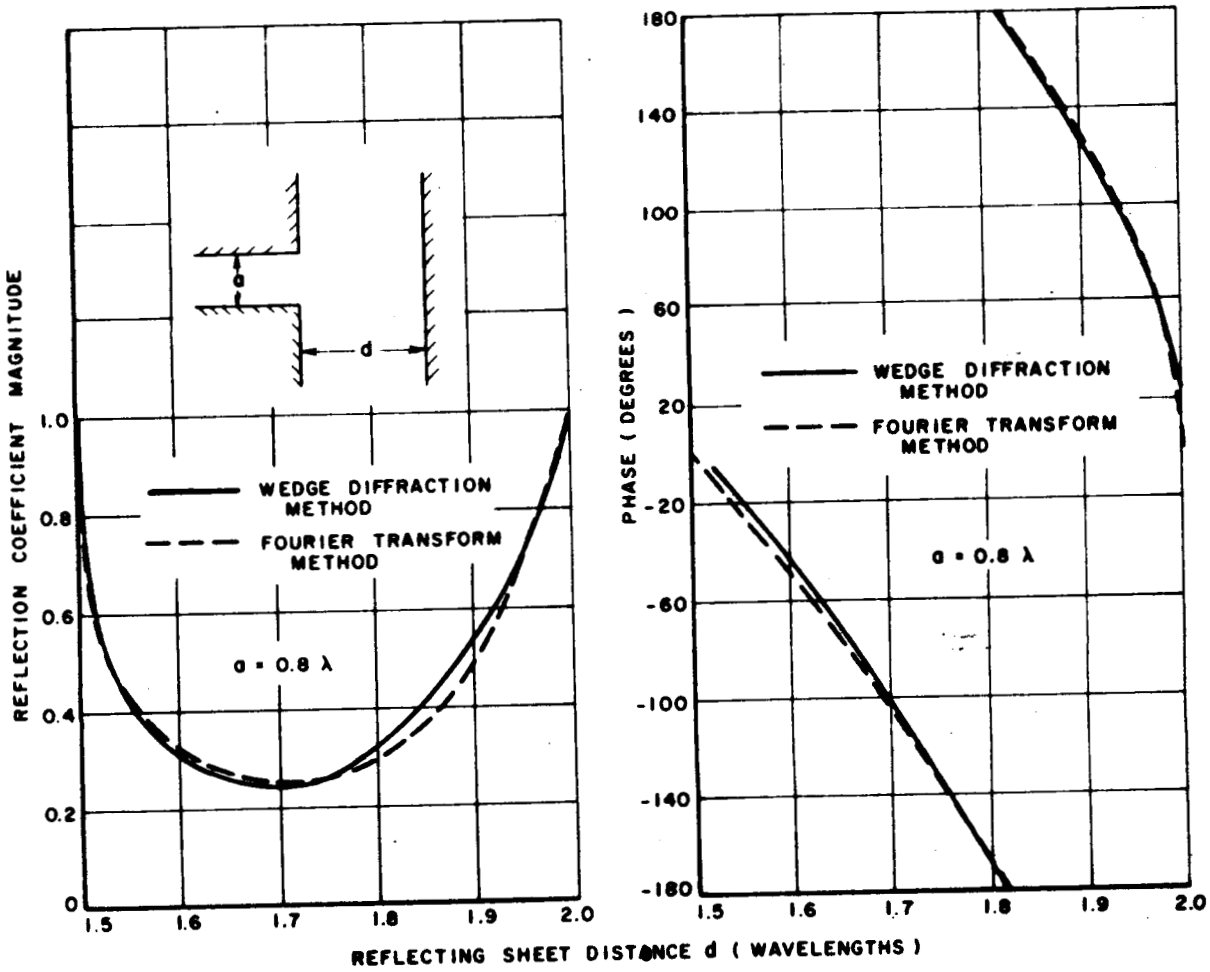

Fig. 15. Reflection coefficient comparison for a = 0.8λ .

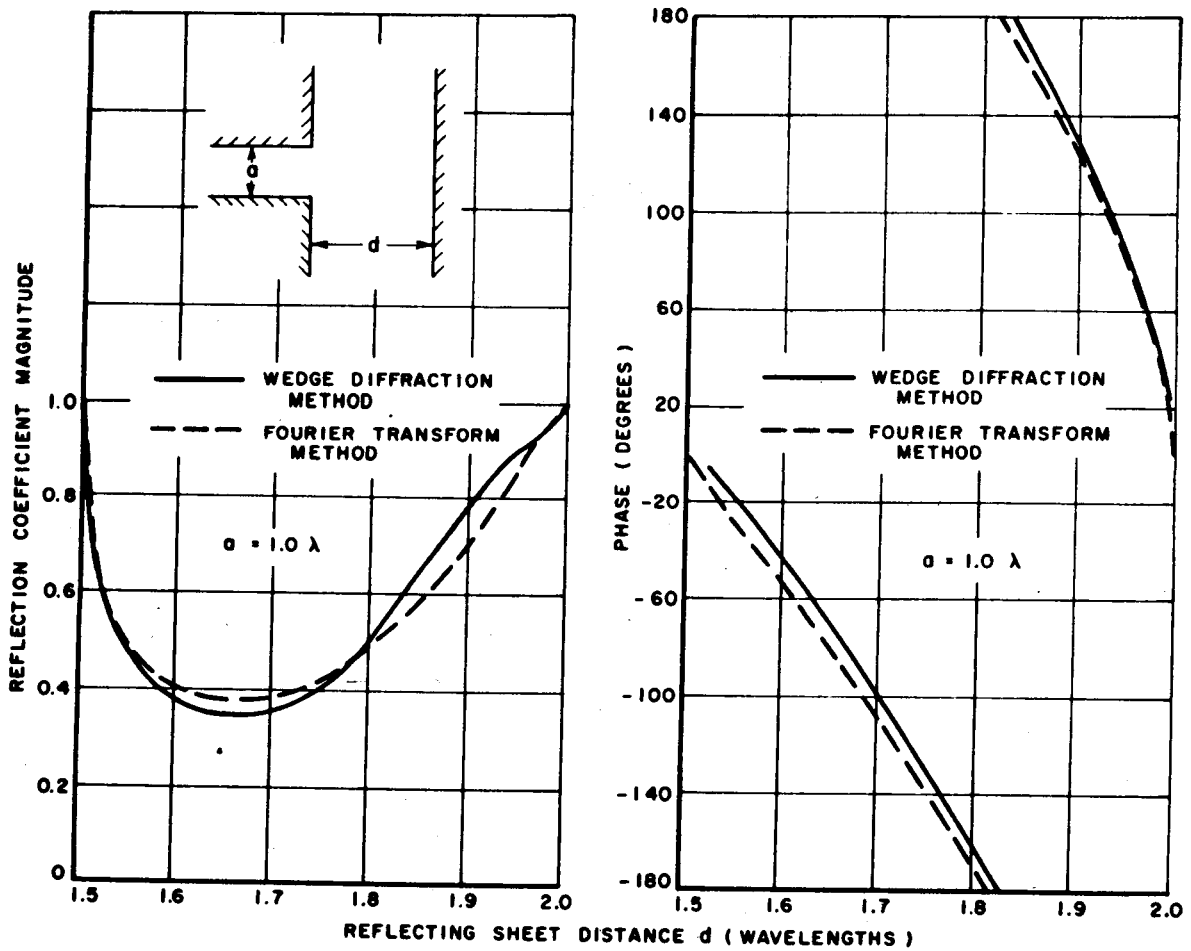

Fig. 16. Reflection coefficient comparison for a = 1.0λ .

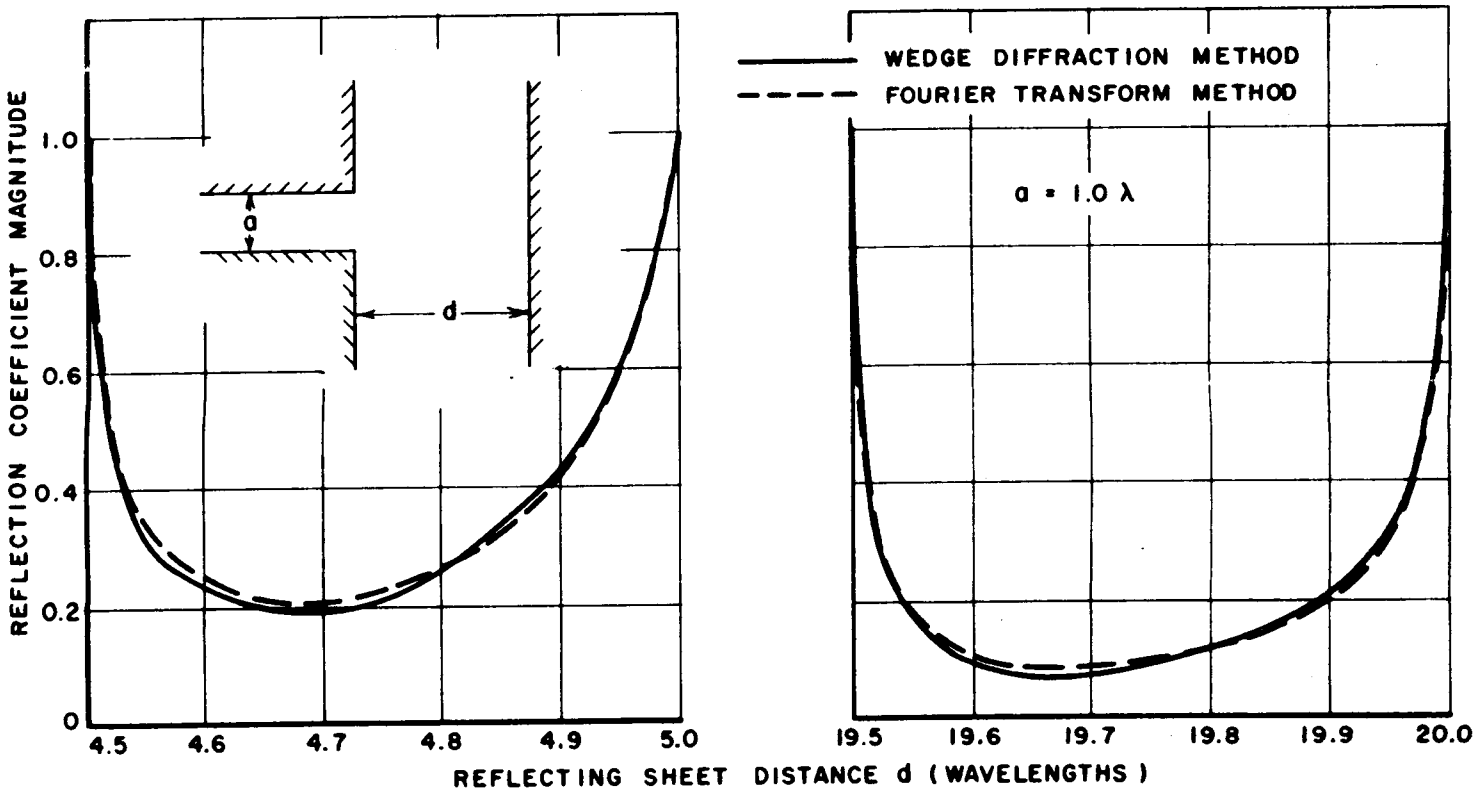

Fig. 17. Reflection coefficient magnitude for a = 1.0λ.

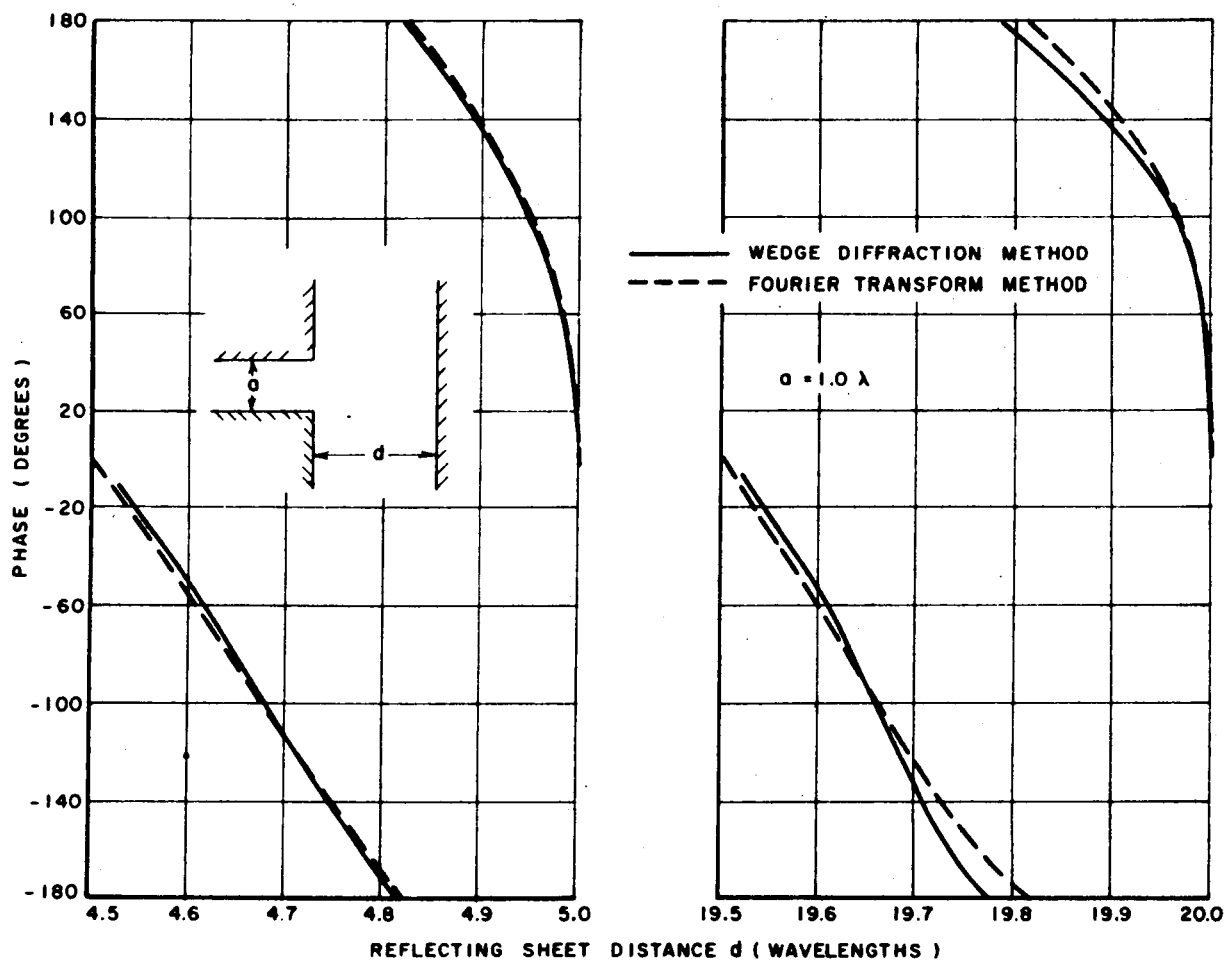

Fig. 18. Reflection coefficient phase for a = 1.0λ .

The resonance behaviors observed at reflector spacings equal to integral multiples of half wavelengths may be further confirmed by examining the Green's function for a magnetic line source located in a parallel-plate region. Morse and Feshback[10] give the Green's function of a source located at (x_o, y_o) as

$$(30) \qquad G(\vec{r}|\vec{r}_o) = \left(\frac{2\pi i}{h}\right) \sum_{\nu=0}^{\infty} \epsilon_\nu \cos\left(\frac{\pi\nu x}{h}\right) \cos\left(\frac{\pi\nu x_o}{h}\right)$$

$$\times \frac{e^{i|y-y_o|\sqrt{k^2-(\pi\nu/h)^2}}}{\sqrt{k^2-(\pi\nu/h)^2}}$$

where h is the cavity spacing.

Kouyoumjian[11] has also obtained the same expression by a different method. It may then be noted that at cavity spacings h equal to integral multiples of half wavelengths, resonance behavior is also observed for a magnetic line source, which may simulate an infinitesimally small TEM mode waveguide.

III. THE TRANSMISSION PROBLEM

A by-product of the above analysis for the reflecting sheet problem shown in Fig. 1 is the solution for the transmission problem shown in Fig. 19. Only the ground plane case (WA = 90°) is considered for the transmission problem. The wave transmitted into the receiving guide is given by summing only the odd-numbered bounces of Eq. (27) and the sum of the even-numbered bounces plus Γ_s gives the reflection coefficient of the transmitting guide.

Representative calculations of transmission and reflection for the transmission problem are given in Figs. 20, 21, and 22 for guide widths equal to 0.278λ and 0.332λ, along with the reflection coefficient for the reflecting sheet problem. It is seen that the transmission peaks occur at every quarter wavelength in d or every half wavelength in the width 2d of the cavity formed between the two ground planes. In the corresponding reflecting sheet problem, the peaks occur at every half wavelength in width d of the cavity formed between the reflecting sheet and the ground plane.

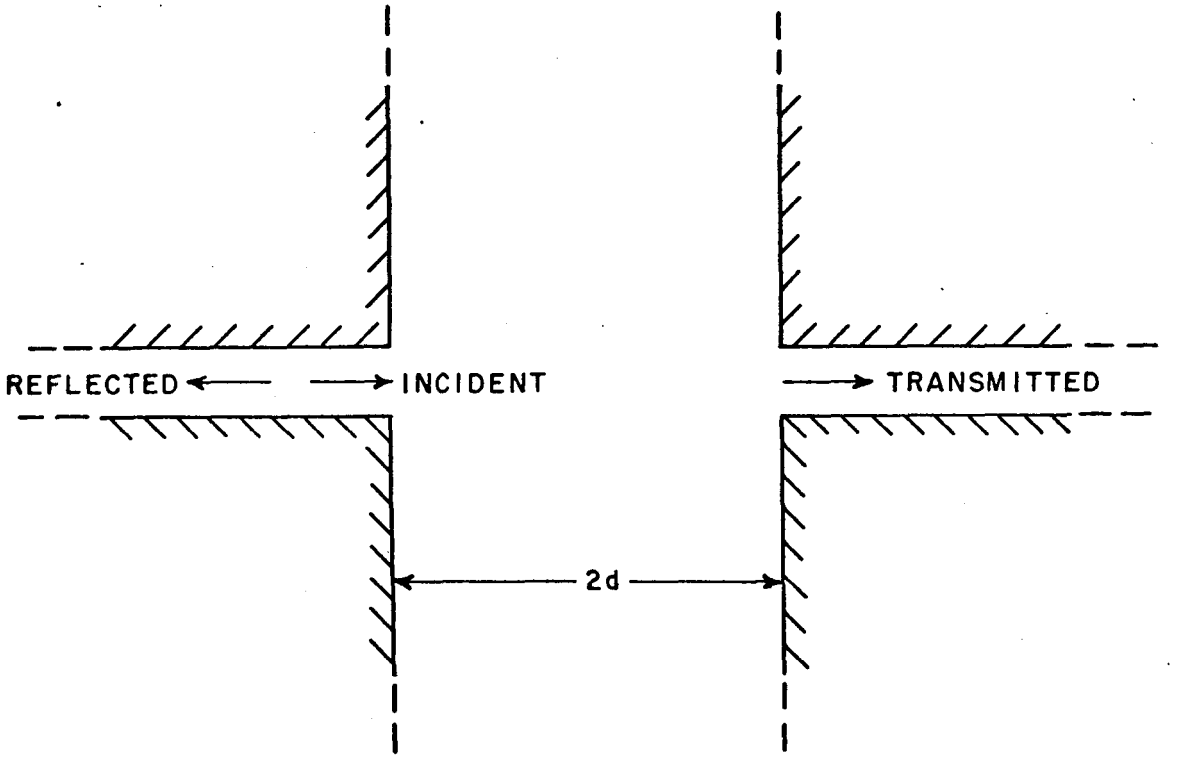

Fig. 19. Transmission between two identical ground-plane mounted parallel-plate waveguides.

Image theory applies to the transmission problem of Fig. 19 when both guides are transmitting equal incident waves and consequently states that the reflection coefficient of each is the same as that for the reflecting sheet problem. This observation provides no additional information since the image problem is essentially identical.

IV. CONCLUSIONS

The reflection coefficient of a TEM mode symmetric parallel-plate waveguide mounted in a ground plane and illuminating a perfectly reflecting sheet has been analyzed by a simplified version of the method in Ref. 1. The simplification allows the practical inclusion of several hundred higher-order interactions. As was shown in Ref. 1, the interaction between the waveguide and reflector can be described in terms of successively bouncing

cylindrical waves. Summation of the contributions of the multiple bounces plus the free space reflection coefficient of the guide yields the total reflection coefficient.

An important physical insight gained by the wedge diffraction analysis is that multiple interactions between the guide and the reflector, i.e., higher order bounce waves, contribute quite significantly to the total reflection coefficient of the waveguide. In fact, at reflector spacings equal to an integral multiple of $\lambda/2$ the reflection coefficient rises to unity magnitude. The results of this analysis agrees well with the Fourier Transform analysis[4] and with measurements.

The wedge diffraction analysis employed in this report for the reflecting sheet problem analyzes cylindrical wave interactions or bounces between the reflecting sheet and the ground plane and thus provides a solution to the transmission between identical waveguides facing each other. This problem is solved by merely summing the odd-numbered and the even-numbered bounces to obtain the transmitted and reflected waves, respectively.

ACKNOWLEDGMENTS

The authors wish to thank Prof. R.G. Kouyoumjian for pointing out the Green's Function solution and to acknowledge Messrs. W.D. Burnside, E.L. Pelton, and D.C.F. Wu for aids rendered in the preparation of this report.

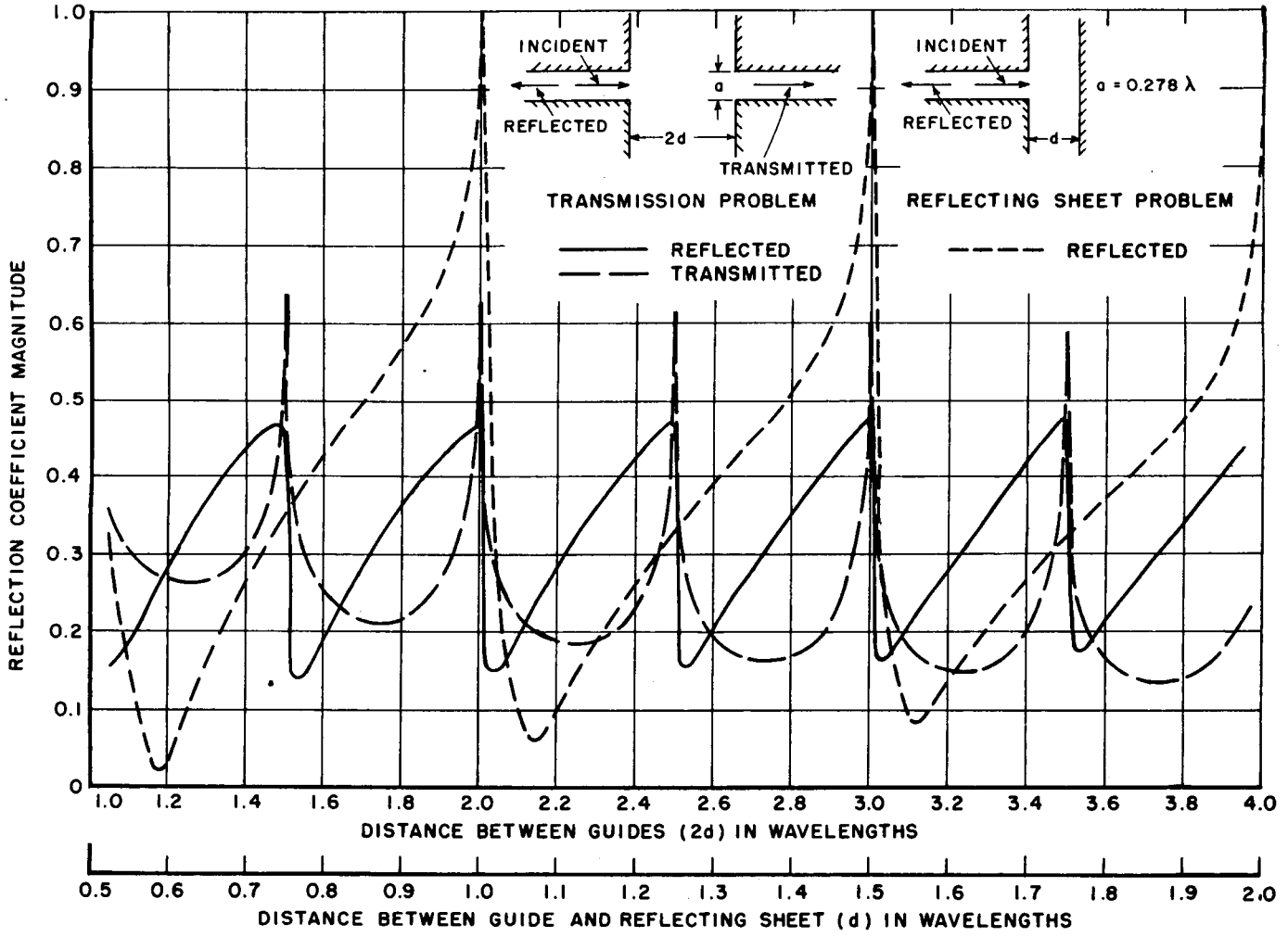

Fig. 20. The transmission problem presented with the reflecting sheet problem for a ground-plane mounted TEM mode parallel-plate waveguide with $a = 0.278\lambda$.

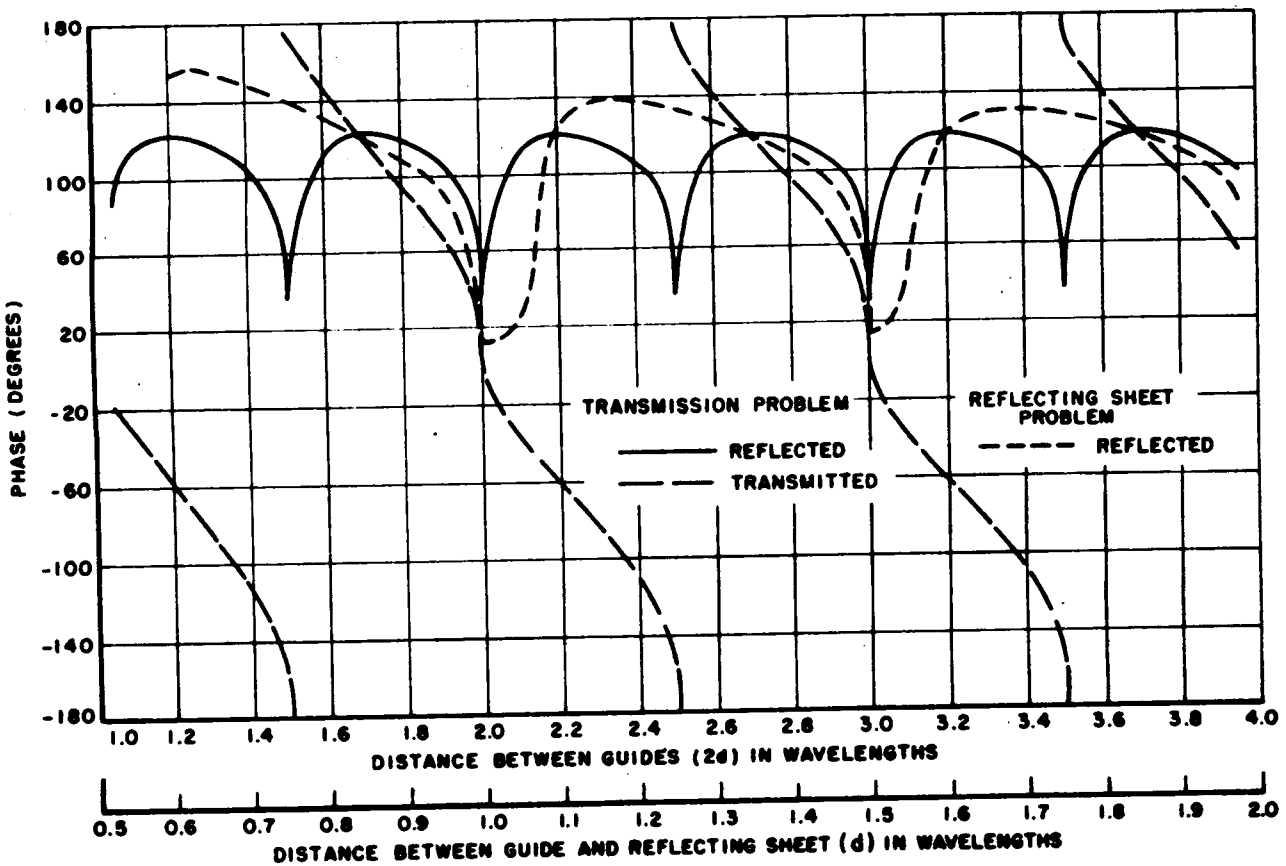

Fig. 21. The transmission problem and the reflecting sheet problem phase.

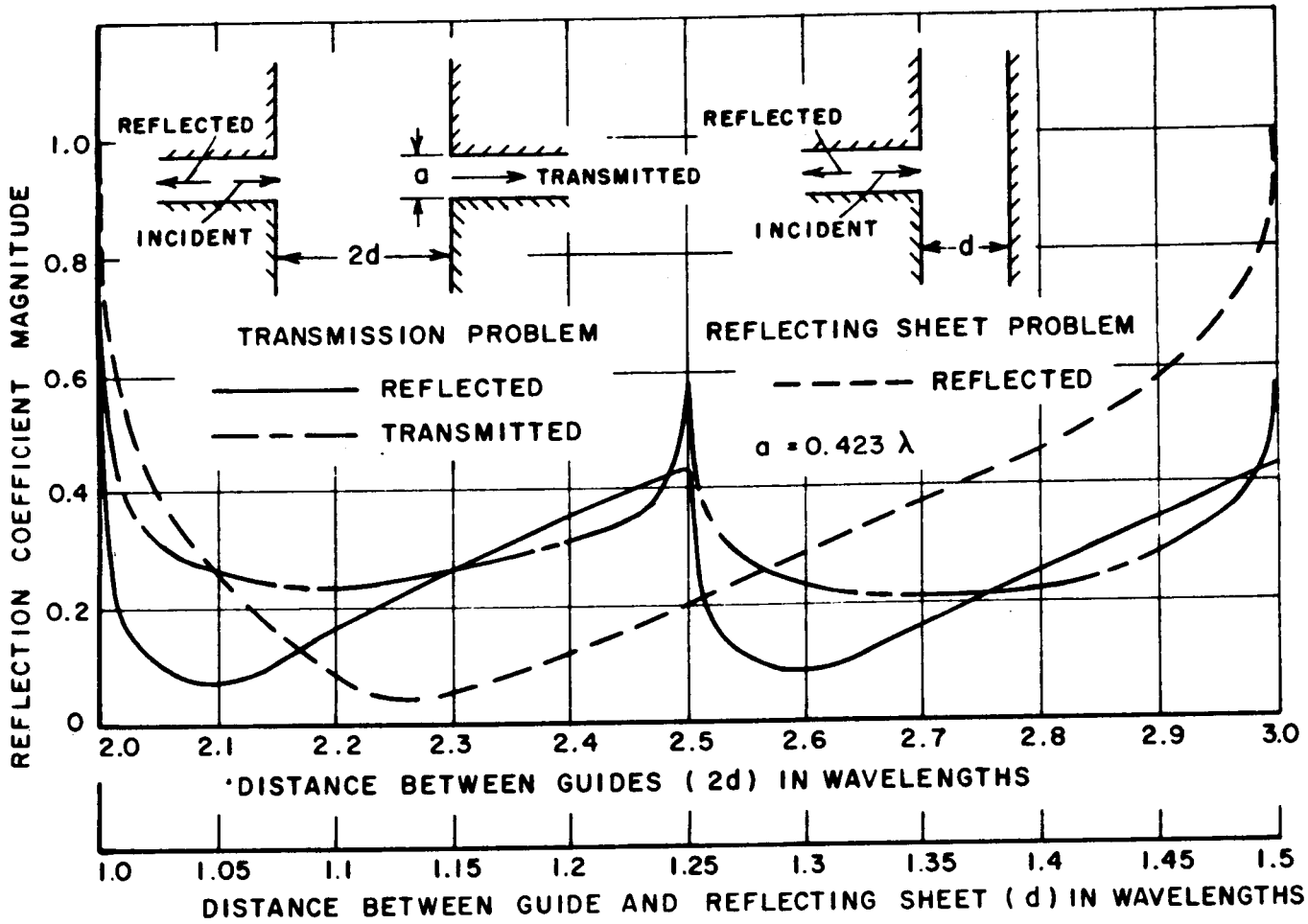

Fig. 22. The transmission problem and the reflecting sheet problem for a = 0.423λ .

APPENDIX I

A Fortran IV program using the OSU-PUFFT Compiler has been written for the computation of the reflection coefficient in Eq. (29). A statement listing is as follows:

```
$EXECUTE        PUFFT
$PUFFT   200
      COMPLEX ABC,CBB
      COMPLEX PPIF,XPIF,GAMS,VB1,VB2,PGAM
      COMPLEX TD0,X,R2,RT,CU,C,GAM,TEM,TEMP
      DIMENSION CUR(500),CUI(500),GAMR(500),GAMI(500)
      PI=3.14159265
      TWP=6.2831853
      PPIF=CEXP(CMPLX(0.,0.7853982))
      XPIF=CONJG(PPIF)
      STWP=SQRT(TWP)
      C1=SIN(TWP/3.0)
      RGTI=-4./3.*C1
      RGTO=-RGTI
      READ (5,13) KC
 13   FORMAT (I2)
      DO 201 KK=1,KC
      READ(5,32) A,GAMS,NC
 32   FORMAT (3F10.5,I2)
      CALL VB (RVB1,UVB1,A,90.0,1.5)
      CALL VB (RVB2,UVB2,A,270.0,1.5)
      VB1=CMPLX(RVB1,UVB1)
      VB2=CMPLX(RVB2,UVB2)
      TD0=RGTO/TWP*XPIF
      X=-A*PPIF-2./(9.*PI)*SQRT(3.)*XPIF+TD0*(VB1+VB2)
      X=X-1.0/1.5*COTAN(2.0943951)/1.5*XPIF/TWP
      R2=RGTI*(VB1+VB2)
      RT=CMPLX(0.0,TWP*A)-COTAN(2.0943951)/1.5+R2
      CU=RT/STWP*CMPLX(0.0,-1.)
      CUR(1)=REAL(CU)
      CUI(1)=AIMAG(CU)
      C=RT/CMPLX(0.0,TWP*A)*PPIF/STWP
      WRITE (6,50) TD0,X,R2
 50   FORMAT (1H ,6E15.7)
      WRITE (6,50) RT,C,CUR(1),CUI(1)
      DO 200 I=1,NC
      READ (5,100) D,NB
 100  FORMAT(F10.5,I5)
      WRITE(6,74)A,D
 74   FORMAT (//1H ,12HGUIDE WIDTH=,F10.5,20X,18HREFLECTOR SPACING=,F10.
     25//)
      WRITE (6,77)
 77   FORMAT(1H ,15HGAMMA INCREMENT,15X,13HGAMMA BOUNCES,17X,11HGAMMA TO
     2TAL/)
      ABC=GAMS
      TD=2.0*D
      GAM=C*CMPLX(CUR(1),CUI(1))/SQRT(TD)*CEXP(CMPLX(0.,-TWP*TD))
      TEM=GAM
      PTEM=180./PI*ATAN2(AIMAG(TEM),REAL(TEM))
      GAMR(1)=REAL(GAM)+REAL(GAMS)
      GAMI(1)=AIMAG(GAM)+AIMAG(GAMS)
      CBB=GAM
      AGAM=SQRT(GAMR(1)**2+GAMI(1)**2)
      PG=180./PI*ATAN2(GAMI(1),GAMR(1))
      N=1
      ATEM=CABS(TEM)
      WRITE (6,29) N,ATEM,PTEM,ATEM,PTEM,AGAM,PG
      DO 200 N=2,NB
      TEMP=CMPLX(0.,0.)
      NM=N-1
      XN=FLOAT(N)
      DO 156 M=1,NM
      XM=FLOAT(M)
      TEMP=X*CMPLX(CUR(M),CUI(M))/SQRT(TD*(XN-XM))*CEXP(CMPLX(0.,-TWP*TD
```

```
     2*(XN-XM)))+TEMP
156   CONTINUE
      CUR(N)=REAL(TEMP)
      CUI(N)=AIMAG(TEMP)
      TEMP=CMPLX(0.,0.)
      XN=FLOAT(N)
      DO 157 M=1,N
      XM=FLOAT(M)
      TEMP=C*CMPLX(CUR(M),CUI(M))/SQRT(TD*(XN-XM+1.))*CEXP(CMPLX(0.,-TWP
     2*TD*(XN-XM+1.)))+TEMP
157   CONTINUE
      GAMR(N)=REAL(TEMP)
      GAMI(N)=AIMAG(TEMP)
      GAMR(N)=GAMR(N)+GAMR(N-1)
      GAMI(N)=GAMI(N)+GAMI(N-1)
      AGAM=SQRT(GAMR(N)**2+GAMI(N)**2)
      PGAM=CMPLX(GAMR(N),GAMI(N))-GAMS
      PTEM=180./PI*ATAN2(AIMAG(TEMP),REAL(TEMP))
      PG=180./PI*ATAN2(GAMI(N),GAMR(N))
      PPG=180./PI*ATAN2(AIMAG(PGAM),REAL(PGAM))
      ATEMP=CABS(TEMP)
      APGAM=CABS(PGAM)
      WRITE (6,29) N,ATEMP,PTEM,APGAM,PPG,AGAM,PG
29    FORMAT (5X,I5,5X,6E15.7)
      XXN=FLOAT (N)
      KHE=N/2
      XXY=XXN/2.0
      XKHE=FLOAT (KHE)
      IF (ABS(XXY-XKHE).GT.0.25) GO TO 573
      ABC=ABC+TEMP
      ABCM=CABS(ABC)
      ABCP=180.0/PI*ATAN2(AIMAG(ABC),REAL(ABC))
      GO TO 937
573   CBB=CBB+TEMP
      CBBM=CABS(CBB)
      CBBP=180.0/PI*ATAN2(AIMAG(CBB),REAL(CBB))
937   WRITE (6,29) N,ATEMP,PTEM,ABCM,ABCP,CBBM,CBBP
200   CONTINUE
201   CONTINUE
      STOP
      END
```

APPENDIX II

The Generalized Pauli Series used in this analysis for the diffraction of a plane wave by a wedge was formulated by Hutchins and Kouyoumjian[8,9] and is presented below. The geometry involved is as shown in Fig. 23.

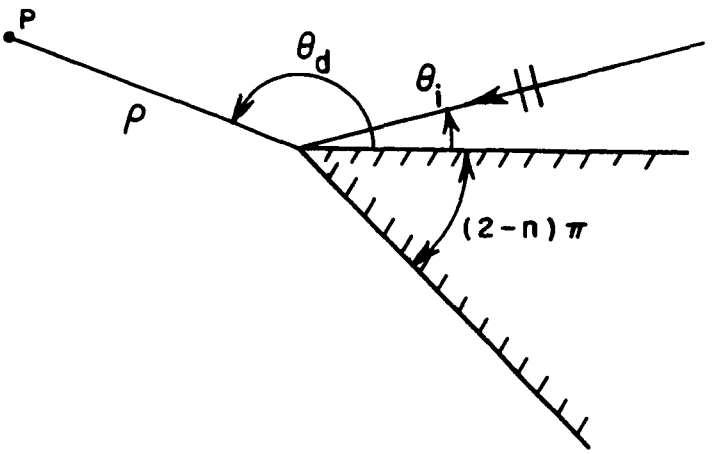

Fig. 23. Plane wave diffraction by a conducting wedge.

The diffracted field is given by

$$U_d(\rho, \theta_i, \theta_d; n) = V_B(\rho, \theta_d - \theta_i, n) \pm V_B(\rho, \theta_d + \theta_i, n) \tag{31}$$

where the + sign is for the electric field polarization perpendicular to the edge of the wedge and the - sign is for the magnetic field polarization perpendicular to the edge of the wedge. The diffraction function V_B is given by

$$V_B(\rho, \beta; n) = I_{-\pi}(\rho, \beta; n) + I_{+\pi}(\rho, \beta, n), \tag{32}$$

where

$$(33) \qquad I_{\pm\pi}(\rho, \beta; n) \sim \frac{e^{-j\left(k\rho + \frac{\pi}{4}\right)}}{jn\sqrt{2\pi}} \sqrt{a} \cot\left(\frac{\pi \pm \beta}{2n}\right)$$

$$\cdot e^{jk\rho a} \int_{(k\rho a)^{\frac{1}{2}}}^{\infty} e^{-j\tau^2} d\tau$$

with

$$a = 1 + \cos(\beta - 2n\pi N),$$

$$\beta = \theta_d \pm \theta_i$$

and N is a positive or negative integer or zero which most nearly satisfies the equations

$$2n\pi N - \beta = -\pi \text{ for } I_{-\pi},$$

$$2n\pi N - \beta = +\pi \text{ for } I_{+\pi} .$$

A Fortran IV program for this V_B function has been written by W.D. Burnside and E.L. Pelton. The Fresnel integral subprogram uses the algorithm found by Boersma.[12] A statement listing of these subprograms is as follows.

```
      SUBROUTINE VB (RVB,UVB,R,ANG,FN)
      COMPLEX DEM,TOP,COM,EXP,UPPI,UNPI
      DOUBLE PRECISION RAG,DP,TSIN
      PI=3.14159265
      TPI=6.28318530
      ANG=ANG*PI/180.0
      DEM=CMPLX(0.0,FN*SQRT(TPI))
      TOP=CEXP(CMPLX(0.0,-(TPI*R+PI/4.0)))
      COM=TOP/DEM
      N=IFIX((PI+ANG)/(2.0*FN*PI)+0.5)
      DN=FLOAT (N)
      A=1.0+COS(ANG-2.0*FN*PI*DN)
      BOTL=SQRT (TPI*R*A)
      EXP=CEXP(CMPLX(0.0,TPI*R*A))
      CALL FRNELS (C,S,BOTL)
      C=SQRT(PI/2.0)*(0.5-C)
      S= SQRT(PI/2.0)*(S-0.5)
      RAG=(PI+ANG)/(2.0*FN)
      TSIN=DSIN(RAG)
      TS=ABS(SNGL(TSIN))
      X=10.0
      Y=1.0/X**5
      IF(TS.GT.Y) GO TO 442
      COMP=-SQRT(2.0)*FN*SIN(ANG/2.0-FN*PI*DN)
      IF(COS(ANG/2.0-FN*PI*DN).LT.0.0) COMP=-COMP
      GO TO 443
  442 DP=SQRT(A)*DCOS(RAG)/TSIN
      COMP=SNGL(DP)
  443 UPPI=COM*EXP*COMP*CMPLX(C,S)
      N=IFIX((-PI+ANG)/(2.0*FN*PI)+0.5)
      DN=FLOAT(N)
      A=1.0+COS(ANG-2.0*FN*PI*DN)
      BOTL=SQRT(TPI*R*A)
      EXP=CEXP(CMPLX(0.0,TPI*R*A))
      CALL FRNELS (C,S,BOTL)
      C=SQRT(PI/2.0)*(0.5-C)
      S= SQRT(PI/2.0)*(S-0.5)
      RAG=(PI-ANG)/(2.0*FN)
      TSIN=DSIN(RAG)
      TS=ABS(SNGL(TSIN))
      IF(TS.GT.Y) GO TO 542
      COMP= SQRT(2.0)*FN*SIN(ANG/2.0-FN*PI*DN)
      IF(COS(ANG/2.0-FN*PI*DN).LT.0.0) COMP=-COMP
      GO TO 123
  542 DP=SQRT(A)*DCOS(RAG)/TSIN
      COMP=SNGL(DP)
  123 UNPI=COM*EXP*COMP*CMPLX(C,S)
      ANG=ANG*180.0/PI
      RVB=REAL (UPPI+UNPI)
      UVB=AIMAG(UPPI+UNPI)
      RETURN
      END
      SUBROUTINE FRNELS(C,S,XS)
      DIMENSION A(12),B(12),CC(12),D(12)
      A(1)=1.595769140
      A(2)=-0.000001702
      A(3)=-6.808568854
      A(4)=-0.000576361
      A(5)=6.920691902
      A(6)=-0.016898657
      A(7)=-3.050485660
      A(8)=-0.075752419
      A(9)=0.850663781
      A(10)=-0.025639041
```

```
      A(11)=-0.150230960
      A(12)=0.034404779
      B(1)=-0.000000033
      B(2)=4.255387524
      B(3)=-0.000092810
      B(4)=-7.780020400
      B(5)=-0.009520895
      B(6)=5.075161298
      B(7)=-0.138341947
      B(8)=-1.363729124
      B(9)=-0.403349276
      B(10)=0.702222016
      B(11)=-0.216195929
      B(12)=0.019547031
      CC(1)=0.0
      CC(2)=-0.024933975
      CC(3)=0.000003936
      CC(4)=0.005770956
      CC(5)=0.000689892
      CC(6)=-0.009497136
      CC(7)=0.011948809
      CC(8)=-0.006748873
      CC(9)=0.000246420
      CC(10)=0.002102967
      CC(11)=-0.001217930
      CC(12)=0.000233939
      D(1)=0.199471140
      D(2)=0.000000023
      D(3)=-0.009351341
      D(4)=0.000023006
      D(5)=0.004851466
      D(6)=0.001903218
      D(7)=-0.017122914
      D(8)=0.029064067
      D(9)=-0.027928955
      D(10)=0.016497308
      D(11)=-0.005598515
      D(12)=0.000838386
      IF(XS.LE.0.0) GO TO 414
      X=XS
      X=X*X
      FR=0.0
      FI=0.0
      K=13
      IF(X-4.0) 10,40,40
10    Y=X/4.0
20    K=K-1
      FR=(FR+A(K))*Y
      FI=(FI+B(K))*Y
      IF(K-2) 30,30,20
30    FR=FR+A(1)
      FI=FI+B(1)
      C=(FR*COS(X)+FI*SIN(X))*SQRT(Y)
      S=(FR*SIN(X)-FI*COS(X))*SQRT(Y)
      RETURN
40    Y=4.0/X
50    K=K-1
      FR=(FR+CC(K))*Y
      FI=(FI+D(K))*Y
      IF(K-2) 60,60,50
60    FR=FR+CC(1)
      FI=FI+D(1)
      C=0.5+(FR*COS(X)+FI*SIN(X))*SQRT(Y)
      S=0.5+(FR*SIN(X)-FI*COS(X))*SQRT(Y)


      RETURN
414   C=-0.0
      S=-0.0
      RETURN
      END
```

APPENDIX III

A shadow boundary approximation of $V_B(\rho, \beta)$ for $\beta \tilde{=} \pi$ as given in Eq. (13) is obtained as follows:

First examine $I_{-\pi}(\rho, \beta, n)$ from Eqs. (32) and (33).

$$(34) \qquad \lim_{\beta \to \pi \pm \epsilon} I_{-\pi}(\rho, \beta, n)$$

$$= \lim_{\beta \to \pi \pm \epsilon} \left\{ \frac{e^{-j\left(k\rho + \frac{\pi}{4}\right)}}{jn\sqrt{2\pi}} \sqrt{a} \cot\left(\frac{\pi - \beta}{2n}\right) e^{jk\rho a} \int_{(k\rho a)^{\frac{1}{2}}}^{\infty} e^{-j\tau^2} \, d\tau \right\}$$

where $a = 1 + \cos\beta \quad (N = 0)$.

Then let us note the following approximations:

$$(35) \qquad \sqrt{a} = \sqrt{1+\cos\beta} = \sqrt{2} \left|\cos\frac{\beta}{2}\right|$$

$$\xrightarrow[\text{as } \beta \to \pi \pm \epsilon]{} \sqrt{2} \left|\cos\left(\frac{\pi}{2} \pm \frac{\epsilon}{2}\right)\right| = \sqrt{2}\left|\sin\frac{\pm\epsilon}{2}\right| \cong \frac{-\sqrt{2}}{2} |\pm\epsilon|$$

for ϵ small

$$(36) \qquad \tan\left(\frac{\pi - \beta}{2n}\right) \xrightarrow[\text{as } \beta \to \pi \pm \epsilon]{} \tan\left(\frac{\pm\epsilon}{2n}\right) = \frac{\sin\left(\frac{\pm\epsilon}{2n}\right)}{\cos\left(\frac{\mp\epsilon}{2n}\right)} \cong \left(\frac{\mp\epsilon}{2n}\right)$$

for ϵ small.

The limiting operation then becomes

$$(37) \qquad \lim_{\beta \to \pi \pm \epsilon} I_{-\pi}(\rho, \beta, n)$$

$$\cong \frac{e^{-j\left(k\rho + \frac{\pi}{4}\right)}}{jn\sqrt{2\pi}} \frac{\frac{\sqrt{2}}{2}|\pm\epsilon|}{\left(\frac{\mp\epsilon}{2n}\right)} \lim_{\beta \to \pi \pm \epsilon} \left\{ e^{jk\rho(1+\cos\beta)} \int_{\sqrt{2k\rho}\left|\cos\frac{\beta}{2}\right|}^{\infty} e^{-j\tau^2} \, d\tau \right\}$$

Employing the small argument approximation for the Fresnel integral, it is seen that

$$(38)\qquad \int_{\sqrt{2k\rho}\left|\cos\frac{\beta}{2}\right|}^{\infty} e^{-j\tau^2}\,d\tau \cong \sqrt{\frac{\pi}{2}}\left(\frac{1}{2} - j\,\frac{1}{2}\right) - \sqrt{2k\rho}\left|\cos\frac{\beta}{2}\right|$$

$$= \frac{\sqrt{\pi}}{2}\left[e^{-j\frac{\pi}{4}} - 4\sqrt{\frac{\rho}{\lambda}}\left|\cos\frac{\beta}{2}\right|\right]$$

Combining the results in Eqs. (35), (36), (37), and (38) we obtain

$$(39)\qquad \lim_{\beta\to\pi\pm\epsilon} I_{-\pi}(\rho,\beta,n)$$

$$\cong \pm\frac{1}{2}\,e^{jk\rho\cos\beta}\left[1 - 4\sqrt{\frac{\rho}{\lambda}}\left|\cos\frac{\beta}{2}\right| e^{j\frac{\pi}{4}}\right]$$

where the plus sign is associated with $\beta = \pi + \epsilon$ and the minus sign is associated with $\beta = \pi - \epsilon$.

Now the same operations may be performed on $I_{+\pi}(\rho,\beta,n)$

$$(40)\qquad \lim_{\beta\to\pi\pm\epsilon} I_{+\pi}(\rho,\beta,n)$$

$$= \lim_{\beta\to\pi\pm\epsilon}\left\{\frac{e^{-j\left(k\rho+\frac{\pi}{4}\right)}}{jn\sqrt{2\pi}}\sqrt{a}\,\cot\left(\frac{\pi+\beta}{2n}\right)e^{jk\rho a}\int_{(k\rho a)^{\frac{1}{2}}}^{\infty} e^{-j\tau^2}\,d\tau\right\}$$

where $a = 1 + \cos(\beta - 2n\pi)$ $(N = 1)$.

For ϵ small, a good approximation would be

$$(41)\qquad a = 1 + \cos(\beta - 2n\pi) \cong 1 + \cos(1-2n)\pi\ ,\ \cot\left(\frac{\pi+\beta}{2n}\right) \cong \cot\frac{\pi}{n}\ .$$

Then

$$(42)\qquad \lim_{\beta \to \pi \pm \epsilon} I_{+\pi}(\rho, \beta, n)$$

$$\cong \frac{e^{-j\left(k\rho + \frac{\pi}{4}\right)}}{jn\sqrt{2\pi}} \sqrt{1 + \cos(1-2n)\pi} \cot\frac{\pi}{n}$$

$$e^{jk\rho[1+\cos(\beta - 2n\pi)]} \int_{\sqrt{k\rho[1+\cos(1-2n)\pi}}^{\infty} e^{-j\tau^2}\, d\tau$$

Employing the large argument asymptotic expansion for the Fresnel integral given by

$$(43)\qquad \int_{x}^{\infty} e^{-j\tau^2}\, d\tau \sim \frac{-j\, e^{-jx^2}}{2x}, \text{ for x large,}$$

and combining the relationships of Eqs. (41) and (42), we find

$$(44)\qquad \lim_{\beta \to \pi \pm \epsilon} I_{+\pi}(\rho, \beta, n)$$

$$\cong -\frac{1}{2n} \cot\frac{\pi}{n} \times \frac{e^{j\left(k\rho\cos\beta - \frac{\pi}{4}\right)}}{\sqrt{2\pi k\rho}} .$$

Hence, the shadow boundary approximation for $V_B(\rho, \beta, n)$ for $\beta \cong \pi$ may be expressed as

$$(45)\qquad V_B(\rho,\beta,n) \cong \frac{1}{2}\exp[jk\rho\cos\beta]$$

$$\times\left\{\pm\left[1-4\,e^{j\frac{\pi}{4}}\sqrt{\frac{\rho}{\lambda}}\left|\cos\frac{\beta}{2}\right|\right]\right.$$

$$\left.-\frac{1}{n}\cot\frac{\pi}{n}\;\frac{e^{-j\frac{\pi}{4}}}{\sqrt{2\pi k\rho}}\right\}\quad,\ \text{for}\ \beta\cong\pi$$

where the + sign is for $\beta > \pi$ and the - sign is for $\beta < \pi$.

The validity of Eq. (45) has been verified by comparison with results obtained from the eigenfunction formulation given by

$$(46)\qquad V_B(\rho,\beta) = \frac{1}{n}\sum_{m=0,\,1}^{\infty}\epsilon_{\frac{m}{n}}\,j^{\frac{m}{n}}\,J_{\frac{m}{n}}(k\rho)\cos\frac{m}{n}\beta\;-\;V^*(\rho,\beta)$$

where V^* is the geometrical optics component given by

$$(47)\qquad V^*(\rho,\beta) = \begin{cases}\exp[jk\rho\cos(\beta+2\pi nN)\\ \qquad \text{if } -\pi < \beta + 2\pi nN < \pi\\ \qquad \text{for } N = 0,\ \pm 1,\ \pm 2\\ 0,\ \text{otherwise.}\end{cases}$$

and $\epsilon_{m/n}$ is Neumann's number. The comparison for typical ranges of ρ and β employed in this report is shown in Tables I and II. Equation (45) can then be seen to be a good shadow boundary approximation whose accuracy increases for decreasing values of $(1 + \cos\beta)k\rho$.

On the shadow boundary, i.e., $\beta = \pi$, V_B is accurately given by

$$(48)\qquad V_B(\rho,\beta=\pi,n) \sim \pm\frac{1}{2}e^{-jk\rho} - \frac{1}{2n}\cot\frac{\pi}{n}\;\frac{e^{-j\left(k\rho+\frac{\pi}{4}\right)}}{\sqrt{2\pi k\rho}}\quad .$$

TABLE I

$V_B(\rho=1.0\lambda, \beta, n=1.5)$

β (in degrees)	Eigenfunction Formulation of V_B according to Eq. (46)	Shadow Boundary Approximation of V_B according to Eq. (45)
170.0	-0.3614917 + j 0.0636647	-0.3631518 + j 0.0672927
175.0	-0.4173982 + j 0.0306760	-0.4174924 + j 0.0300565
176.0	-0.4291918 + j 0.0220558	-0.4293600 + j 0.0211283
177.0	-0.4411354 + j 0.01266105	-0.4414378 + j 0.0115609
178.0	-0.4531978 + j 0.0024462	-0.4536685 + j 0.0012868
179.0	-0.4653436 - j 0.0086347	-0.4659914 - j 0.0097629
180.0^-	-0.4775324 - j 0.0206277	-0.4783417 - j 0.0216582
180.0^+	0.5224676 - j 0.0206277	0.5216583 - j 0.0216582
181.0	0.5102809 - j 0.0326225	0.5093494 - j 0.0335120
182.0	0.4981415 - j 0.0437082	0.4971506 - j 0.0444371
183.0	0.4860898 - j 0.0539315	0.4851258 - j 0.0545027
184.0	0.4741612 - j 0.0633381	0.4733345 - j 0.0637767
185.0	0.4623868 - j 0.0719734	0.4618322 - j 0.0723250
190.0	0.4066414 - j 0.1050881	0.4103997 - j 0.1062834

TABLE II

$V_B(\rho = 3.0\lambda, \beta, n = 1.5)$

β (in degrees)	Eigenfunction Formulation of V_B according to Eq. (46)	Shadow Boundary Approximation of V_B according to Eq. (45)
170.0	-0.2992610 + j 0.0963678	-0.3196212 + j 0.1153991
175.0	-0.3848230 + j 0.0640383	-0.3864326 + j 0.0668182
176.0	-0.4042744 + j 0.0530977	-0.4049357 + j 0.0544522
177.0	-0.4243764 + j 0.0402138	-0.4245673 + j 0.0406628
178.0	-0.4450208 + j 0.0251690	-0.4450639 + j 0.0251363
179.0	-0.4660657 + j 0.0077345	-0.4661435 + j 0.0075329
180.0^-	-0.4873291 - j 0.0123277	-0.4874955 - j 0.0125045
180.0^+	0.5126709 - j 0.0123277	0.5125045 - j 0.0125045
181.0	0.4914107 - j 0.0323876	0.4912241 - j 0.0324696
182.0	0.4703744 - j 0.0498169	0.4703585 - j 0.0498561
183.0	0.4497428 - j 0.0648551	0.4502139 - j 0.0650171
184.0	0.4296558 - j 0.0777343	0.4310662 - j 0.0782865
185.0	0.4102195 - j 0.0886765	0.4131695 - j 0.0899702
190.0	0.3247258 - j 0.1211227	0.3506759 - j 0.1323250

APPENDIX IV

The free-space reflection coefficient of a ground-plane mounted parallel-plate waveguide was analyzed by wedge difffraction and compared to results from other methods of analysis in Ref. 3. The comparison showed close agreement in the reflection coefficient magnitude. The comparison in reflection coefficient phase is shown in Fig. 24. The result of Harrington[13] is essentially that from a Fourier Transform solution with a dominant mode assumption. Do Amaral and Bautista Vidal[14] included the effects of higher-order modes in a variational solution. The Geometrical Theory of Diffraction (GTD) results were obtained by Yee, Felsen and Keller.[15] The phase correction factor introduced by the presence of higher order modes is thus demonstrated by this comparison.

It is believed that the presence of higher order modes will enter into the reflection coefficient analysis of this report in another regard, i.e., the on-axis radiation from the free-space guide as depicted in Fig. 25. Calculations of the on-axis field employing a variational expression with a dominant mode assumption[13] has been performed. A detailed comparison of this result with that obtained from wedge diffraction analysis will be given in Ref. 6. In general, however, close agreement is found in the magnitude but some phase differences (on the order of 10° for a guide width of 0.278λ) is noted. It is believed that the presence of higher order modes causes this phase deviation in a manner similar to that for the free-space reflection coefficient.

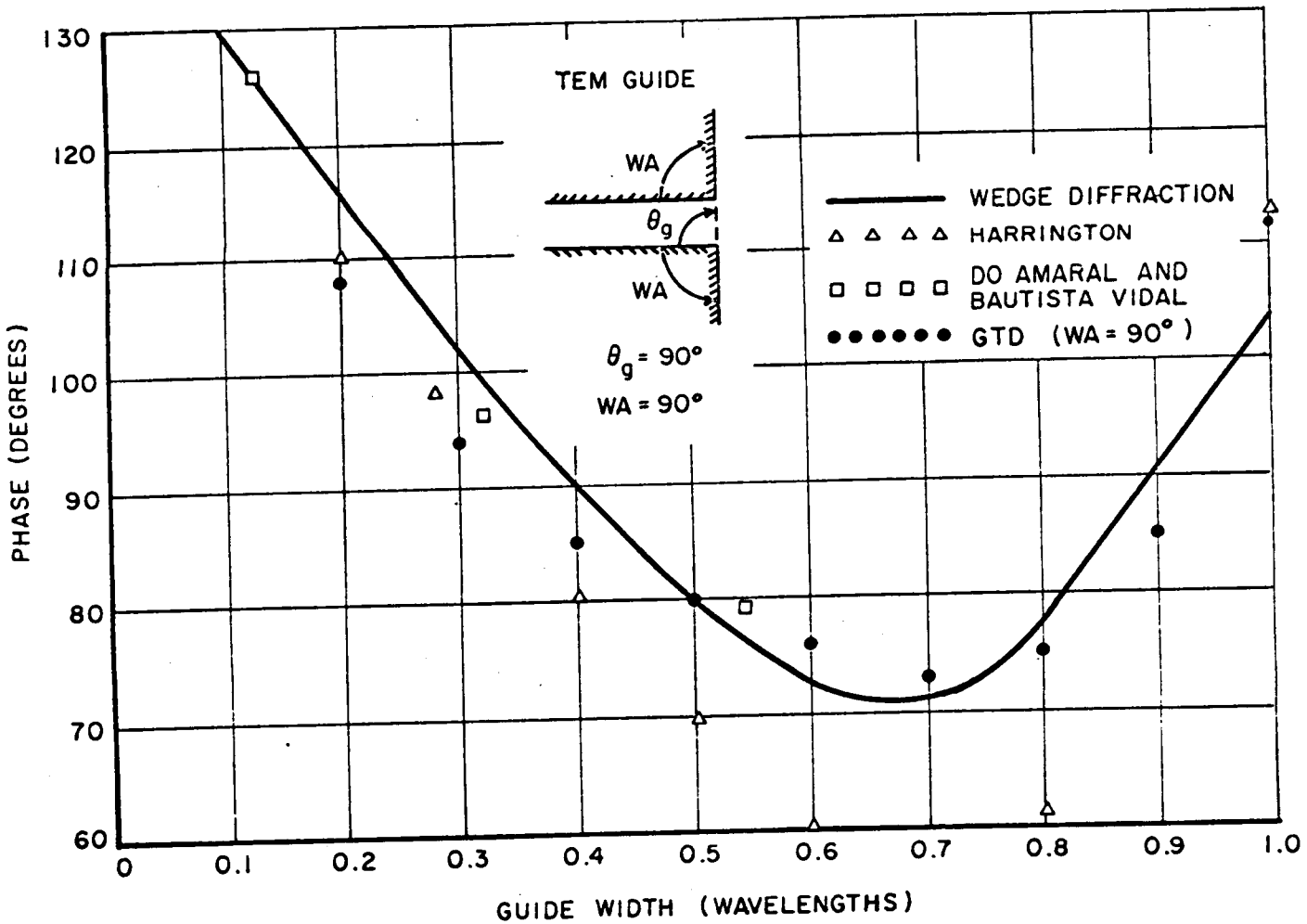

Fig. 24. TEM reflection coefficient phase.

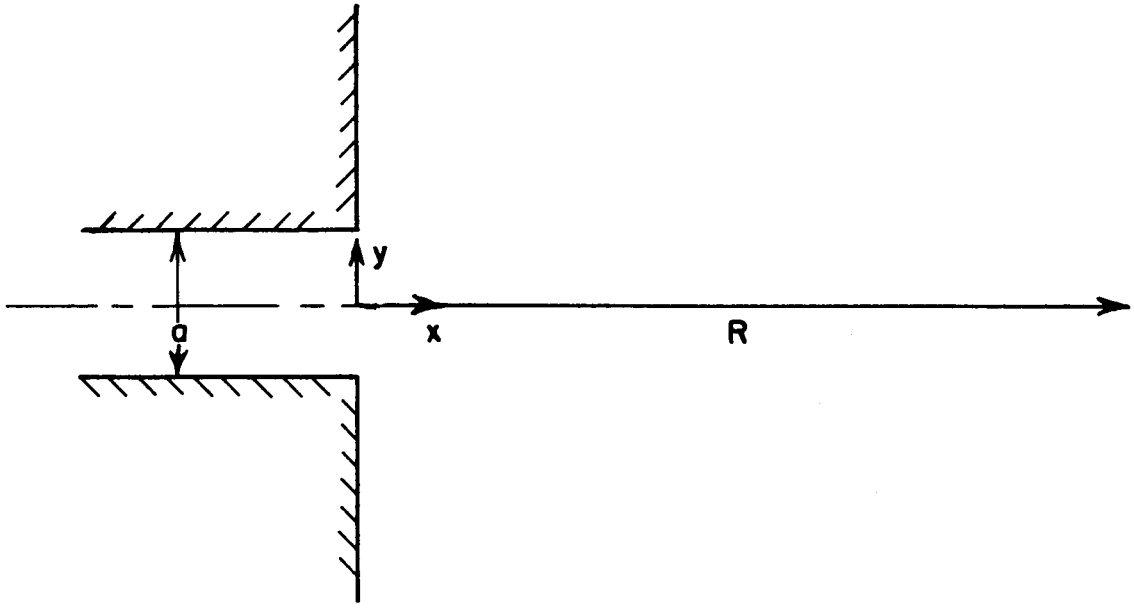

Fig. 25. On-axis field.

REFERENCES

1. Tsai, L.L., "The Reflection Coefficient of a TEM Mode Parallel-Plate Waveguide Illuminating a Perfectly Reflecting Sheet," Report 2143-1, 25 August 1966, Antenna Laboratory, The Ohio State University Research Foundation; prepared under Grant NGR-36-008-048, National Aeronautics and Space Administration, Office of Grants and Research Contracts, Washington, D.C.

2. Burnside, W.D., Tsai, L.L., and Rudduck, R.C., "The Reflection Coefficient of a TEM Mode Parallel-Plate Waveguide Illuminating a Conducting Sheet - the Large Wedge Angle Case," Report 2143-2, 2 February 1968, ElectroScience Laboratory, The Ohio State University Research Foundation; prepared under Grant NGR-36-008-048, National Aeronautics and Space Administration, Office of Grants and Research Contracts, Washington, D.C.

3. Rudduck, R.C., and Tsai, L.L., "Aperture Reflection Coefficient of TEM and TE_{01} Mode Parallel-Plate Waveguides," IEEE Transactions on Antennas and Propagation, Vol. AP-16, No. 1, (January 1968), pp. 83-89.

4. Jones, J. Earl, and Swift, C.T., "The Aperture Admittance of a Ground Plane-Mounted Waveguide Illuminating a Perfectly Conducting Sheet," NASA TN L-5645, Langley Research Center, Hampton, Va.

5. Dybdal, R.B., Rudduck, R.C., and Tsai, L.L., "Mutual Coupling Between TEM and TE_{01} Parallel-Plate Waveguide Aperture," IEEE Transactions on Antennas and Propagation, Vol. AP-14, No. 5, (September 1966), pp. 574-580.

6. Wu, D.C.F., Tsai, L.L., and Rudduck, R.C., "Broadside Radiation of Parallel-Plate Waveguides," (Report in preparation).

7. Pauli, W., "An Asymptotic Series for Functions in the Theory of Diffraction of Light," Phys. Rev., 54, (1 December 1938), pp. 924-931.

8. Hutchins, D.L., and Kouyoumjian, R.G., "A New Asymptotic Solution to the Diffraction by a Wedge," URSI 1967 Spring Meeting; Ottawa, Canada, pp. 154-155.

9. Hutchins, D.L., "Asymptotic Series Describing the Diffraction of a Plane Wave by a Two-Dimensional Wedge of Arbitrary Angle," PhD Dissertation, The Ohio State University Electrical Engineering Department, (1967).

10. Morse, P.H., and Feshback, H., Methods of Theoretical Physics, McGraw-Hill, New York, N.Y., (1953), pp. 814-820.

11. Kouyoumjian, R.G., The Ohio State University, Columbus, Ohio, private communications.

12. Boersma, J., "Computation of Fresnel Integrals," Math. Comp. Vol. 14, (1960), p. 380.

13. Harrington, R.F., Time-Harmonic Electromagnetic Fields, McGraw-Hill Book Company, Inc., New York (1961), pp. 180-185.

14. Do Amaral, C. Marcio and J.W. Bautista Vidal, "Evanescent Mode Effects in the Double-Wedge Problem," Appl. Sci. Res., Section B, Vol. 11, (January 1963), pp. 1-25.

15. Yee, H.Y., Felsen, L.B., and Keller, J.B., "Ray-Optical Calculations of Reflection from an Open-Ended Waveguide," URSI 1967 Spring Meeting, Ottawa, Canada, pp. 175-176.